IEEE Access
Multidisciplinary : Rapid Review : Open Access Journal

Received 17 September 2022, accepted 3 October 2022, date of publication 10 October 2022, date of current version 17 October 2022.

Digital Object Identifier 10.1109/ACCESS.2022.3213713

RESEARCH ARTICLE

Electronically Tunable 3D Autonomous Chaotic Oscillator Employing Single CCCFA and Its Extension to 4D

GARIMA SHUKLA AND SAJAL K. PAUL
Department of Electronics Engineering, Indian Institute of Technology (ISM), Dhanbad 826004, India
Corresponding author: Sajal K. Paul (sajalkpaul@rediffmail.com)

ABSTRACT This work presents the realization of a novel electronically tuneable third-order autonomous chaotic oscillator using a current-controlled current conveyor feedback amplifier (CCCFA). The proposed circuit consists of a single CCCFA, two grounded passive capacitors, one inductor, and two diodes. The chaotic oscillator possesses smooth symmetrical sin-hyperbolic nonlinearity through two antiparallelly connected diodes. The electronically tunable intrinsic resistance at the X terminal serves as the bifurcation control parameter in the circuit and is controlled through bias current. Tuning of bias current enables the formation of different periodic and chaotic attractors. The proposed chaotic oscillator exhibits rich nonlinear dynamical behavior such as periodicity, antimonotonicity, and coexistence of attractors. Multistability is investigated through circuit-level simulation. The chaotic oscillator can easily be implemented in an integrated circuit as the configuration is simple, resistorless, and uses the minimum number of components in the count. Further, a higher dimensional (4D) chaotic oscillator is proposed as an extended circuit of the 3D chaotic oscillator and illustrated as an application in chaos encryption. Simulations are done using TSMC 180nm CMOS technology in PSpice. Experimental results are presented to verify the theoretical and simulation analyses of the proposed circuits.

INDEX TERMS 3D, 4D, autonomous, CCCFA, chaotic, electronic tuneability, multistability, oscillator.

I. INTRODUCTION

At present, nonlinear chaotic systems contribute a captivating gateway into the world of chaos research. In the past few years, chaotic oscillator designs have received rising attention due to chaotic signal's possible commercial applications, mainly in secured communication systems, EEG signal analysis, cryptography, and many more [1], [2]. In the current scenario, analog IC designers have extended the traditional dynamical system designs to a high-performance design in terms of low power consumption, wider bandwidth, simple circuitry, and suitability for VLSI integration. Some basic chaos generators using non-autonomous and autonomous chaotic oscillator circuits are classical Chua's circuit [3], [4], [5], jerk circuit [6], and autonomous oscillator [7].

The continuous improvements of chaotic oscillator designs have attracted considerable attention. Previous chaotic system designs have been based on different realizations using an operational amplifier (Op-amp)/current feedback operational amplifier (CFOA) [3], [4], [8], [9], [10], [11], [12], [13], [14], [15], [16], [17], [18]. The most realized configuration in chaotic oscillator design is classical Chua's oscillator [3], [4], which has served as the guide for most implementations. Further, the different chaotic oscillators have been derived from conventional sinusoidal oscillators and other configurations [8], [9], [10], [11], [12], [13], [14], [15], [16], [17], [18]. It can be inferred that the most challenging part of synthesizing a chaotic circuit is the design of active nonlinearity [4], [5], [6], [7], [8], [9], [10], [11], [12], [13], [14], [15], [16], [17], [18]. Nonlinearity is categorized broadly in two forms; asymmetric and symmetric. Most chaotic oscillators' initial realizations comprise asymmetric and segmented piecewise nonlinearity. In [14], [15], [16], [17], and [18], Chaotic oscillators have

The associate editor coordinating the review of this manuscript and approving it for publication was Ludovico Minati.

been designed with asymmetric nonlinearity, whereas Op-amp and CFOA-based oscillators in [3], [4], [19], [20], [21], and [22] comprise segmented piecewise nonlinearity.

The segmented piecewise nonlinear function is non-smooth and non-differentiable; hence it has been substituted with various smooth nonlinear functions. The presence of a smooth symmetric function yields a circuit capable of rich and exciting nonlinear behaviors. The smooth nonlinear functions used for designs are arbitrary polynomial [23], Jerk function [24], and conically shaped functions [25]. Chua's circuit implements a cubic nonlinearity in [26], [27], [28], and [29]. In [26], cubic-like nonlinearity is generated through cubic polynomial realization. The transistor-level nonlinearity generated in [27], [28], and [29] resulted in an approximation of cubic-like nonlinearity. However, designs reported in [23], [24], [25], and [26] reveal that implementations of exactly smooth nonlinear functions need several analog multipliers and voltage mode building blocks powered with high supply voltages, and very high active and passive components count, making the resulting circuit very complex. Designs [27], [28], [29] present an approximation of smooth nonlinearity; hence do not exhibit advanced dynamical phenomena such as periodicity, anti-monotonicity, and coexistence of attractor [30], [31].

Further, transistor-based chaotic oscillators are reported in [32], [33], [34], and [35]. Two transistors-based chaotic oscillator is presented in [32]; however, it possesses many limitations, such as an excessive number of resistors in the circuit, the asymmetry between upper and lower bands of double scroll attractors due to different average collector current of the transistor, and limited oscillation frequency in kHz. The existence of chaos in a second-order transistor-based oscillator is presented in [33]; however, the oscillator is nonautonomous and does not employ symmetric nonlinearity. Hence cannot generate double scroll attractors and advanced dynamical behavior. The transistor-based Colpitts and Hartley oscillators have been modified for chaos in [34] and [35]; however, these oscillators do not possess symmetric nonlinearity, and behavior is limited up to the formation of single scroll attractors. Moreover, these circuits cannot exhibit advanced dynamical phenomena, e.g., multistability and antimonotonicity, and are not able to generate complex double scroll attractors.

Furthermore, the high-frequency chaos generators for VHF/UHF communication have been illustrated in [36], [37], and [38]. A vacuum tube-based delayed feedback klystron chaotic oscillator is presented in [36]. Reference [37] presents a spin wave transmission line based chaos generator, and [38] presents a micro-stripline chaos generator. These generators produce chaotic oscillations in the high-frequency range from MHz to GHz. However, implementation of these generators is complex and very bulky as; chaos is controlled through electron beams [36], the efficiency of generated chaos is affected by the attenuation losses of spin wave transmission line [37], and the dimensionality of chaos generator depends on the dimension of micro strip transmission line [38]. Moreover, power consumption in these generators is very high.

The simplicity of a chaotic oscillator may be assessed in terms of three major criteria as follows: (a) simple mathematical equations involving nonlinear function for smooth and symmetric nonlinearity, (b) simple circuitry employing minimum possible active/passive components, and (c) easy practical implementation using off the shelf ICs. Therefore, because of the simplest chaotic oscillator circuit design with smooth symmetric nonlinearity, the literature [13], [39], [40], [41], [42], [43], [44] illustrated the use of two antiparallelly connected diodes generating sin-hyperbolic like smooth symmetric nonlinearity. The chaotic oscillator in [39] uses one CFOA, two capacitors, one inductor, one resistor, and two diodes, whereas the circuit in [40] uses one Op-Amp, two capacitors, one inductor, three resistors, and two diodes. The chaotic oscillator in [41] uses one Op-Amp, two capacitors, one inductor, one resistor, and two diodes.

During the past few decades, the current-mode approach in analog integrated circuit design has been receiving enormous attention over its voltage mode counterparts due to their potential advantages, such as inherently wide bandwidth, higher slew rate, greater linearity, wider dynamic range, simple circuitry, and low power consumption [14], [20], [21], [22], [25], [45], [46], [47]. Chaotic oscillator in [45] uses one current mode block, namely an operational trans-resistance amplifier (OTRA), two capacitors, one inductor, two resistors, and two diodes, whereas [46] uses one CFOA, one inverter, two capacitors, one inductor, one resistor, and two diodes. However, it is revealed from [39], [40], [41], [45], [46] that designs use an excessive number of components and/or do not possess advanced dynamical behaviors.

One of the desirable phenomena in current mode circuit design is the feature of electronic tuneability using intrinsic resistance of the current mode building block (CMBB). Chaotic oscillator designs having electronic tuneability features are reported in a few of the literature [16], [24]; however, none of them possesses the tunability through electronically controlled intrinsic resistance of the employed active block, which serves as the main bifurcation control parameter in the circuit. The chaotic oscillator in [16] employs electronic tuneability through external bias current to control the bifurcation parameter in the circuit, whereas tuneability in [24] is achieved through transconductance of the active block. Moreover, tunability for chaos control in chaotic systems is also achieved through techniques like adaptive symmetry and control [48], [49], hybrid synchronization in synchronized hybrid generators [50], and backstepping control [51]. In these techniques, the chaotic behavior of the system is controlled through adaptive control of symmetry coefficient or bifurcation parameters. However, tuneability in these techniques is achieved through synchronization between two chaotic systems; therefore, these techniques involve two chaotic systems either identical or one analog and another discrete to generate complex and random behaviour.

Moreover, it is known [39], [40], [41], [45], [46] that many analog 3D chaotic oscillators have limitations in providing some complex dynamic behaviors like complex phase portraits, a high degree of unpredictability, a complex chaotic regime for a wide range of control parameters, and a high degree of secure transmission. However, this statement is not precisely true, especially for digital or hybrid chaos generators based on minimal discrete chaotic maps, adaptive symmetry [48], and synchronized hybrid chaos generation with hybrid synchronization [50]. These characteristics can be achieved by a higher-dimensional analog chaotic oscillator like 4D. Considerable numbers of analog 4D chaotic oscillators have been designed in the literature [42], [43], [44], [45], [46], [47], [52], [53], [54], [55], [56], [57], [58], and references cited therein. The topologies [42], [43], [44], [47], [52], [53], [54], [55], [56], [57], [58] realize only a 4D chaotic oscillator; however, [45], [46], as discussed in the previous paragraph, realize 3D and then extend to 4D. The reported 4D oscillators possess one or more of the following shortcomings: non-availability of smooth symmetric nonlinearity/non-formation of complex attractors in all planes/use of excessive numbers of ABBs/use of multipliers/use of excessive passive components/non-availability of intrinsic electronic tuning.

An exhaustive literature survey motivated the authors to propose a novel, simple chaotic oscillator configuration with minimum possible active and passive components and advanced chaotic phenomena features. The proposed chaotic oscillator is resistorless and employs a single current mode CMOS-based building block, CCCFA, with two capacitors, one inductor, and two diodes. The circuit is electronically tuneable with the intrinsic resistance (R_X) at the X terminal of CCCFA, which serves as the bifurcation parameter, on being controlled through bias current. Further, a higher dimensional (4D) chaotic circuit is realized by simply adding one capacitor and one resistor as an extension of the proposed 3D chaotic oscillator to illustrate the more complex dynamical behavior. An application of chaos encrypted ECG signal for secured communication in 3D, and 4D oscillators is provided.

This paper is organized into various sections. Section 1 is this section; herein, an introduction is given. Section 2 presents the proposed third-order chaotic oscillator (3D), followed by Section 3 wherein illustrates the dynamical analysis. Section 4 presents the simulation results and discussion. In section 5, phenomena of antimonotonicity and coexisting attractors are presented. Section 6 presents the extended 4D chaotic oscillator and its simulation results. Section 7 illustrates the application of proposed chaotic circuits in chaos encryption. Section 8 shows the experimental results, followed by Section 9, wherein a comparison is given. Section 10 is the conclusion.

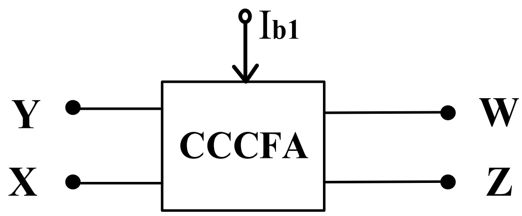

(a)

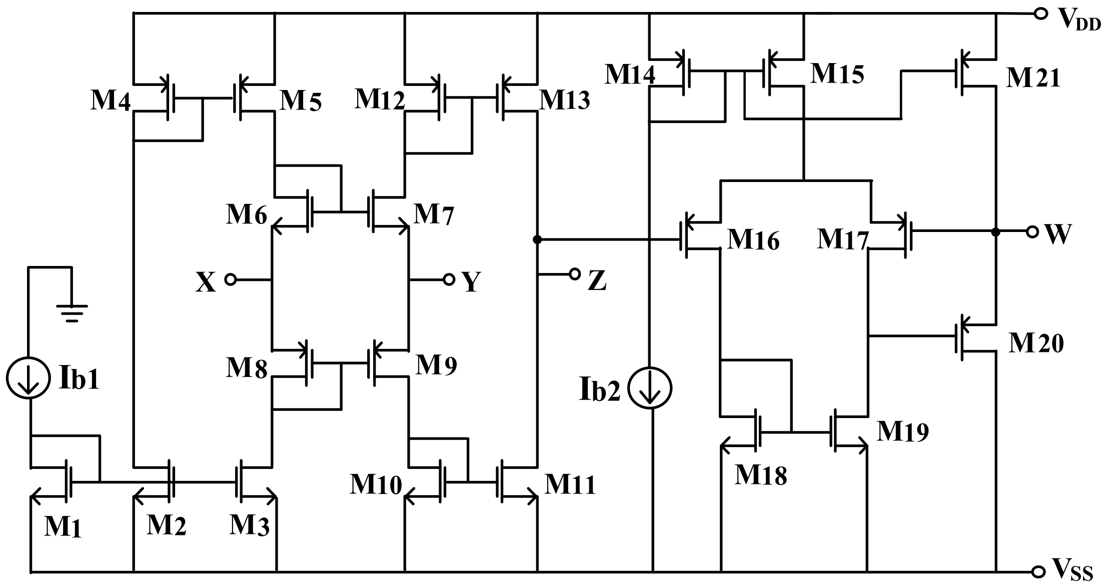

(b)

FIGURE 1. CCCFA (a) symbolic representation (b) CMOS realization.

II. CHAOTIC OSCILLATOR USING A SINGLE CCCFA

This section proposes a new autonomous chaotic oscillator using a single CCCFA, two diodes, and a few passive components.

A. CURRENT CONTROLLED CURRENT CONVEYOR FEEDBACK AMPLIFIER (CCCFA)

The current feedback operational amplifier (CFA or CFOA) is one of the most versatile active blocks in current mode circuit designs. The structure of CFOA combines a second-generation current conveyor (CCII) and a buffered amplifier (BA) [59], [60]. There are various CMOS-based CFOAs available in the literature [59], [60]. However, CFOAs do not possess the electronic tuneability feature. Therefore, CCCFA [61], [62], [63] has been proposed to offer electronic tuneability in CFOAs. In CCCFA, electronically tunable intrinsic resistance (R_X) at the X terminal is available, which is controlled through tuning of bias current [61], [62], [63]. CCCFA combines a second-generation current controlled current conveyor (CCCII) and a BA [61], [62], [63]. This paper presents a fully CMOS-based structure of CCCFA. The symbolic representation of the CCCFA is shown in Fig. 1(a). The CMOS realization of CCCFA is shown in Fig. 1(b), combining the CCCII [63] formed of M_1-M_{13} and a BA [59] formed of M_{14}-M_{21}. R_X is controlled through bias current, I_{b1}. Port relationships are as follows:

$$\begin{pmatrix} I_Y \\ V_X \\ I_Z \\ V_W \end{pmatrix} = \begin{pmatrix} 0 & 0 & 0 & 0 \\ R_X & 1 & 0 & 0 \\ 1 & 0 & 0 & 0 \\ 0 & 0 & 1 & 0 \end{pmatrix} \begin{pmatrix} I_X \\ V_Y \\ V_Z \\ V_W \end{pmatrix} \tag{1}$$

where in (1),

$$R_X = \frac{1}{\sqrt{8kI_{b1}}} \tag{2}$$

where, $k = \mu_n C_{OX}\left(\frac{W}{L}\right)_{6,7} = \mu_p C_{OX}\left(\frac{W}{L}\right)_{8,9}$.

B. PROPOSED CHAOTIC OSCILLATOR

The proposed third-order autonomous chaotic oscillator is shown in Fig. 2. A chaotic oscillator is derived from a conventional sinusoidal oscillator by connecting a nonlinear element/composite in the configuration [64]. In the proposed circuit, a passive LC resonator formed by L and C_1 is connected to antiparallelly connected diodes through an active RC network formed by CCCFA, R_X, and C_2. The C_1-L-C_2 configuration with CCCFA forms a linear third-order sinusoidal oscillator, and diodes are used to induce the nonlinear behavior. CCCFA with R_X acts as a NIC (negative impedance converter) to make the circuit satisfy the necessary oscillation condition. Electronically controllable intrinsic resistance, R_X, serves as a bifurcation control parameter and is tuned through bias current, I_{b1}, to result in different nonlinear chaotic phenomena.

The dynamics of the proposed 3D chaotic oscillator are described by a mathematical model, which is defined in a set of three first-order autonomous differential equations as;

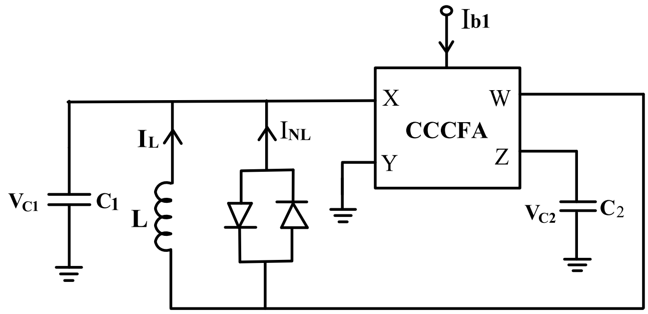

FIGURE 2. Proposed chaotic oscillator circuit.

$$C_1\frac{dV_{C2}}{dt} = -V_{C1}\sqrt{8kI_{b1}} + I_{NL} + I_L;$$
$$C_2\frac{dV_{C1}}{dt} = -V_{C1}\sqrt{8kI_{b1}}, \quad L\frac{dI_L}{dt} = V_{C2} - V_{C1} \tag{3}$$

From (2) and (3), the model equations result as follows:

$$C_1\frac{dV_{C2}}{dt} = -\frac{V_{C1}}{R_X} + I_{NL} + I_L; \quad C_2\frac{dV_{C1}}{dt} = -\frac{V_{C1}}{R_X};$$
$$L\frac{dI_L}{dt} = V_{C2} - V_{C1} \tag{4}$$

where V_{C1} and V_{C2} are the voltages across capacitors C_1 and C_2, respectively. I_L is the current in the inductor, L. I_{NL} corresponds to the nonlinear current of two antiparallel diodes, having sin-hyperbolic like characteristics, and is obtained as;

$$I_{NL} = I_{D1} - I_{D2} = I_S e^{\left(\frac{V_{diff}}{V_r}\right)-1} - I_S e^{\left(-\frac{V_{diff}}{V_r}\right)-1}$$
$$= 2I_S \sinh\left(\frac{V_{diff}}{V_r}\right) \tag{5}$$

where, $V_{diff} = V_{C2} - V_{C1}$, $V_r = \eta V_T$, thermal voltage, $V_T = 26mV$ at room temperature, and I_S is the reverse saturation current of the diode.

Further, (4) is represented in the form of a standard jerk equation [24] of a third-order chaotic oscillator as;

$$\frac{d^3V_{C2}}{dt^3}LC_1C_2R_X + \frac{d^2V_{C2}}{dt^2}LC_1 + \frac{dV_{C2}}{dt}R_XC_1 + V_{C2} + f_{NL} = 0 \tag{6}$$

where f_{NL} is the nonlinear function of I_{NL}.

Dynamic properties and other measures of chaos are examined through the analytical method to verify that the system's flow (3) is chaotic. For this, (3) is transformed into dynamic state equations having a set of dimensionless variables (x, y, and z) and control parameters (β, a, b, and φ). The transformed state equations result as;

$$\dot{x} = -ax + z + \varphi\sinh(y - x)$$
$$\dot{y} = -abx$$
$$\dot{z} = y - x \tag{7}$$

where $\dot{x}$, $\dot{y}$, and $\dot{z}$ are the derivatives of x, y, and z, respectively, with respect to τ. Moreover,

$$x = \frac{V_{C1}}{V_r}, \quad y = \frac{V_{C2}}{V_r}, \quad z = \frac{\beta I_L}{V_r}, \quad a = \beta\sqrt{8kI_{b1}} = \frac{\beta}{R_X},$$

$$b = \frac{C_1}{C_2}, \quad \beta = \sqrt{\frac{L}{C_1}}, \ \varphi = \frac{2aI_S}{V_r}, \quad \text{and } t = \tau\sqrt{LC_1} \tag{8}$$

Based on (7) and (8), numerical and simulation analyses of the proposed circuit are discussed in sections 3 and 5.

III. DYNAMICAL ANALYSIS

A. SYMMETRY AND INVARIANCE

System (7) is invariant, for co-ordinate substitution (x, y, z) ⇔ (−x, −y, −z). If (x, y, z) is the solution of the system, then (−x, −y, −z) is also a solution for the same set of parameter values. The two trajectories have symmetry, and origin (0, 0, 0) is the equilibrium point and a trivial static solution of (7).

B. EXISTENCE OF ATTRACTORS

The existence of developed attractors in the designed system (7) is verified by calculating the volume (V) contraction/expansion rate of the system at any given point of the state space [30], [31]. For verification of this, divergence (∇) of the system (7) is found and is obtained as;

$$\nabla V = \frac{\delta\dot{x}}{\delta x} + \frac{\delta\dot{y}}{\delta y} + \frac{\delta\dot{z}}{\delta z} \tag{9}$$

On solving (7) using (9), we get

$$\nabla V = -a - \varphi\cosh(y - x) < 0 \tag{10}$$

The value of '$-\varphi\cosh(y-x)$' at any given point (x, y) in the state space will always be negative. Therefore, it confirms from (10) that $-a - \varphi\cosh(y - x) < 0$, i.e., the divergence of the system will always be less than zero anywhere in state space. It verifies that system (7) is dissipative. $\nabla V < 0$ reflects that the initial volume of state space of (7) will be contracted endlessly, and the convergence of asymptotic motion of all orbits settles to an attractor.

C. FIXED POINT ANALYSIS

The chaotic system's complex dynamics are attained by investigating the equilibrium state's stability [30], [31]. System (7) has a single equilibrium point or fixed point at the origin (0, 0, 0); hence eigenvalues for the system at (0, 0, 0) are calculated. For this, the Jacobian matrix (M_J) of (7) is obtained at any arbitrary point of coordinate (x, y, z) as;

$$M_J = \begin{pmatrix} -a - \varphi\cosh(y-x) & \varphi\cosh(y-x) & 1 \\ -ab & 0 & 0 \\ -1 & 1 & 0 \end{pmatrix} \tag{11}$$

Consequently, the eigenvalues of the matrix (11) at the origin (0, 0, 0) are found by solving the characteristic equation as;

$$\det(M_J - \lambda I) = 0 \tag{12}$$

where 'I' is a 3 × 3 identity matrix.

Since the eigenvalues are calculated at the equilibrium point i.e. origin (0,0,0), therefore the term '$\cosh(y-x)$' for x=0, y=0 results in unity. Hence, on considering $\cosh(y - x) = 1$ in (11), the characteristic equation from (11) and (12), results as;

$$\lambda^3 + \lambda^2(a + \varphi) + \lambda(1 + ab\varphi) + ab = 0 \tag{13}$$

As an example, considering the control parameters, (a, b) = (1.12, 50) and $\varphi = 0.58{*}10^{-4}$, the corresponding eigenvalues evaluated at the origin from (13) are obtained as $\lambda_1 = -4.1422$, $\lambda_{2,3} = 1.511 \pm j3.3519$. Outcome $\lambda_{2,3}$ indicates that the origin is unstable in the chaotic regime due to the presence of a positive real part in the eigenvalue. This is the characteristic of a self-excited chaotic oscillatory system.

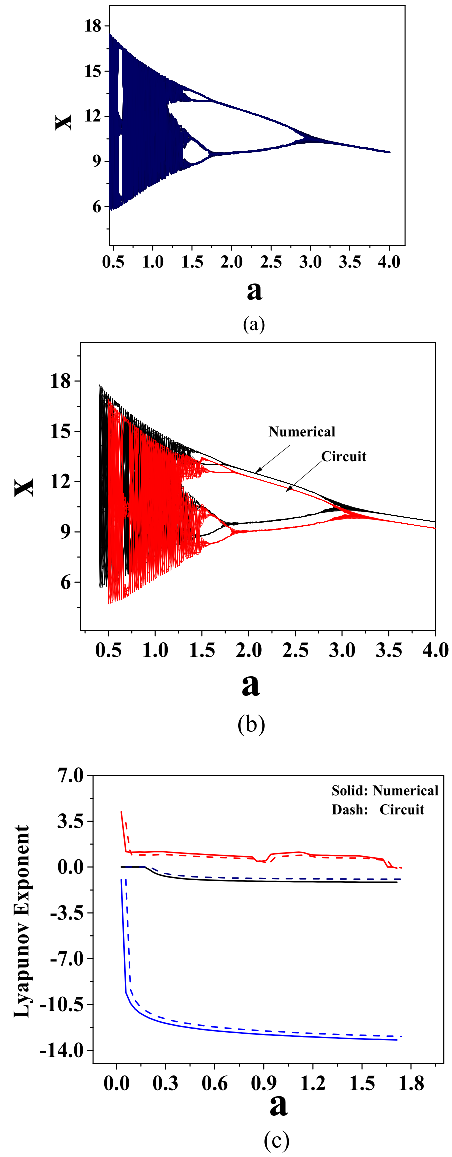

FIGURE 3. Plot for (a) bifurcation of 'a' vs. 'x'. (b) bifurcation plots from circuit and numerical simulation (c) lyapunov exponent vs. 'a'.

D. BIFURCATION

Further, to observe the effect of bifurcation control parameter 'a' on the system (7) and to measure the transition to chaos, the bifurcation diagram is shown in Fig. 3(a), which has

TABLE 1. Aspect ratio of transistors in CCCFA.

Transistor	W(um)	L(um)
M_1–M_3, M_6, M_7, M_{10}, M_{11}, M_{18}, M_{19}	18	0.36
M_4, M_5, M_8, M_9, M_{12}, M_{13}	36	0.36
M_{16}, $M1_7$	36	0.36
M_{14}, M_{15}, M_{20}, M_{21}	25	0.36

been plotted numerically in MATLAB. For fixed parameters (b=50, $\beta = 0.8944^*10^3$), 'a' is varied, and the corresponding 'x' is obtained without resetting the initial condition. Fig. 3(a) shows the development of a rich bifurcation process indicating local maxima for 'x' over a range of 'a'. Moreover, the bifurcation diagram is plotted for the circuit's acquired data, obtained from multiple time series responses of the proposed circuit in PSpice, and is compared with numerically simulated responses, as shown in Fig. 3(b). It is observed that the response obtained from the circuit's acquired data is in close agreement with the response obtained through numerical simulation. However, slight shift in diagrams is due to the two different integration schemes employed in numerical and circuit simulations i.e., Runge-Kutta in MATLAB and implicit integration in PSpice.

E. ROUTE TO CHAOS

To attain additional proof of chaoticity, the Lyapunov exponents are obtained. The values of the Lyapunov exponent less than zero correspond to regular motions, while positive values correspond to chaotic states. The Lyapunov exponents of the designed system (7) are plotted in MATLAB with the standard Runge-Kutta integration scheme for fixed parameters (b=50, $\beta = 0.8944^*10^3$) and compared with the values obtained from the circuit's acquired data. As shown in Fig 3(c), the largest positive Lyapunov exponent is 1.48 (red color); this confirms the proposed oscillator's chaotic behavior.

IV. SIMULATION RESULTS FOR THE CHAOTIC OSCILLATOR

The chaotic oscillator is simulated using TSMC 0.18μm CMOS process technology in PSpice with technology model parameters as; $C_{OX} = 8.422\text{fF}/\mu\text{m}^2$, $\mu_{O(N)} = 259.53\text{cm}^2/\text{V-s}$, $\mu_{O(P)} = 109.97\text{cm}^2/\text{V-s}$, and $t_{OX} = 4.1$nm. The results are obtained for parameter values as; $V_{DD} = -V_{SS} = 3$V, $I_{b2} = 10\mu$A, $C_1 = 50$pF, $C_2 = 1$pF, $L = 40$uH, and $I_{b1} = 148\mu$A to 195μA. The aspect ratio of transistors in CCCFA is shown in Table 1.

The simulated time-domain responses of V_{C1} and V_{C2} of the chaotic oscillator of Fig. 2 for different values of I_{b1} (i.e., R_X) are depicted in Fig. 4(a)-(d). It is observed in Fig. 4(a)-(d) that on the tuning of I_{b1}, the circuit produces rich and interesting nonlinear behaviors of V_{C1} and V_{C2}. Further, the phase portraits of V_{C1} vs. V_{C2} signals are shown in Fig. 5(a)-(i) for varying bias current, I_{b1}. The phase trajectories of a single period, period-2, and period-4, are obtained, as shown in Fig. 5(a)-(c) for the I_{b1} of 195μA, 189μA, and 184μA, respectively. The single-scroll attractor is obtained for $I_{b1} = 171\mu$A, as shown in Fig. 5(d), followed by the double scroll attractor through bifurcation for $I_{b1} = 164\mu$A, as shown in Fig. 5(e). On further decreasing I_{b1}, single scroll, period-4, period-2, and single period are obtained at 154.7μA, 151μA, 148μA, and 144μA, respectively, as shown in Fig. 5(f)-(i). Fig. 5(f)-(i) depict similar types of attractors as that of Fig. 5(a)-(d), but the direction of trajectories is different.

Similarly, different phase portraits of V_{C2} versus I_L for different I_{b1} are shown in Fig. 6(a)-(h). The phase trajectories of a single period, period-2, and period-4, are obtained, as shown in Fig. 6(a)-(c) for the I_{b1} of 195μA, 189μA, and 184μA, respectively. The single-scroll attractor is obtained for $I_{b1} = 171\mu$A, as shown in Fig. 6(d), followed by the double scroll attractor formed for $I_{b1} = 164\mu$A, as shown in Fig. 6(e). On further decreasing I_{b1}, single scroll, period-4, period-2, and single period are obtained at 154.7μA, 151μA, 148μA, and 144μA, respectively, as shown in Fig. 6(f)-(i). Further, different phase portraits of V_{C1} versus I_L are obtained, as shown in Fig. 7(a)-(d). The phase trajectories of single period and period-2 attractors are shown in Fig. 7(a) and (b) for I_{b1} of 195μA and 189μA, respectively. The single-scroll attractor is obtained at $I_{b1} = 171\mu$A, as shown in Fig. 7(c), and the double scroll attractor is obtained at $I_{b1} = 164\mu$A, as shown in Fig. 7(d).

Further, the frequency spectrum of chaotic oscillations for V_{C1} and V_{C2} are shown in Fig. 8(a) and 8(b), respectively. The proposed circuit exhibits high-frequency chaotic oscillations as Fig. 8(a) and (b) depict; the dominant operating frequency of chaotic oscillation corresponds to 8.4MHz. However, it is also verified to operate over a wide frequency range of 18 kHz to 16.8 MHz (not shown).

V. ADVANCED DYNAMICAL PHENOMENA

A. ANTIMONOTONICITY

An interesting nonlinear phenomenon that has been investigated in symmetric dynamical systems is antimonotonicity. This measures the richness of the chaotic system and is the concurrent formation of forward periodic orbits, and then their destruction via a reverse period-doubling as a bifurcation control parameter is slowly monitored [30]. It should be noted that to exhibit this phenomenon, a nonlinear system must have the presence of periodic orbits in the parameter space as obtained in Fig. 5(a)-(c), (g)-(i). As expressed in (8), 'a' is a bifurcation control parameter tuned through I_{b1}. For system (7), 'a' varies in the range, $0.5 \leq a \leq 3.2$, and correspondingly bifurcations for V_{C2} are plotted. Bifurcations are shown in Fig. 9(a)-(c) for a single period, period-2, and double scroll attractor, respectively, for $\beta = 0.8944^*10^3$ and different values of b.

B. COEXISTING ATTRACTORS AND MULTISTABILITY

One of the most striking phenomena in symmetric chaotic system designs is finding various regions in the control

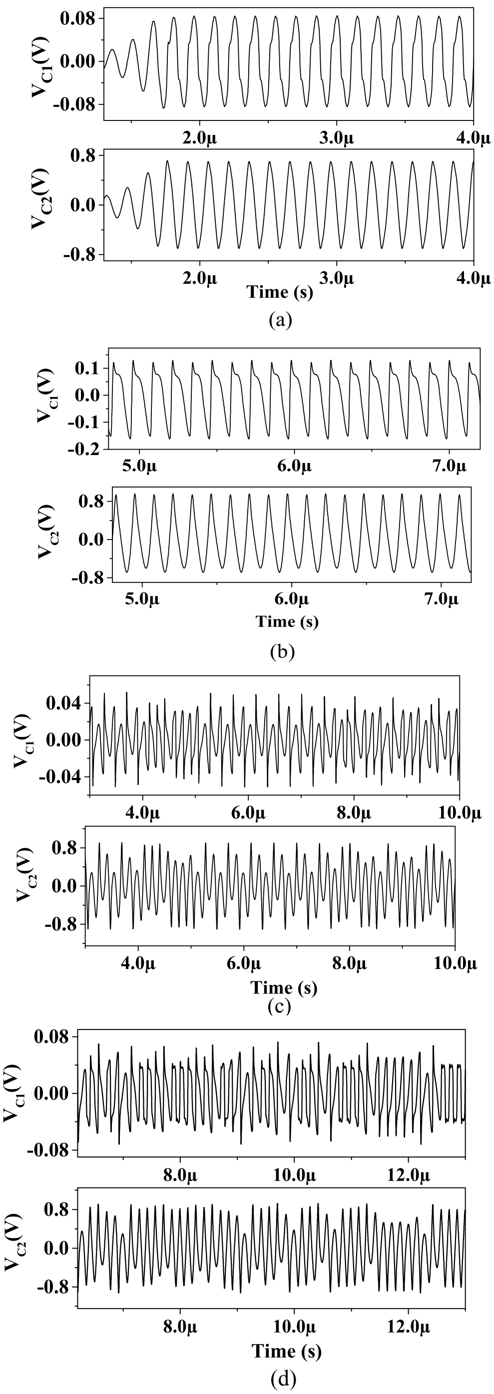

FIGURE 4. Time domain responses; (a) single period (I_{b1}=195μA (b) period-2 ((I_{b1}=189μA) (c) single scroll (I_{b1}=171μA) (d) double scroll attractor ((I_{b1}=164μA).

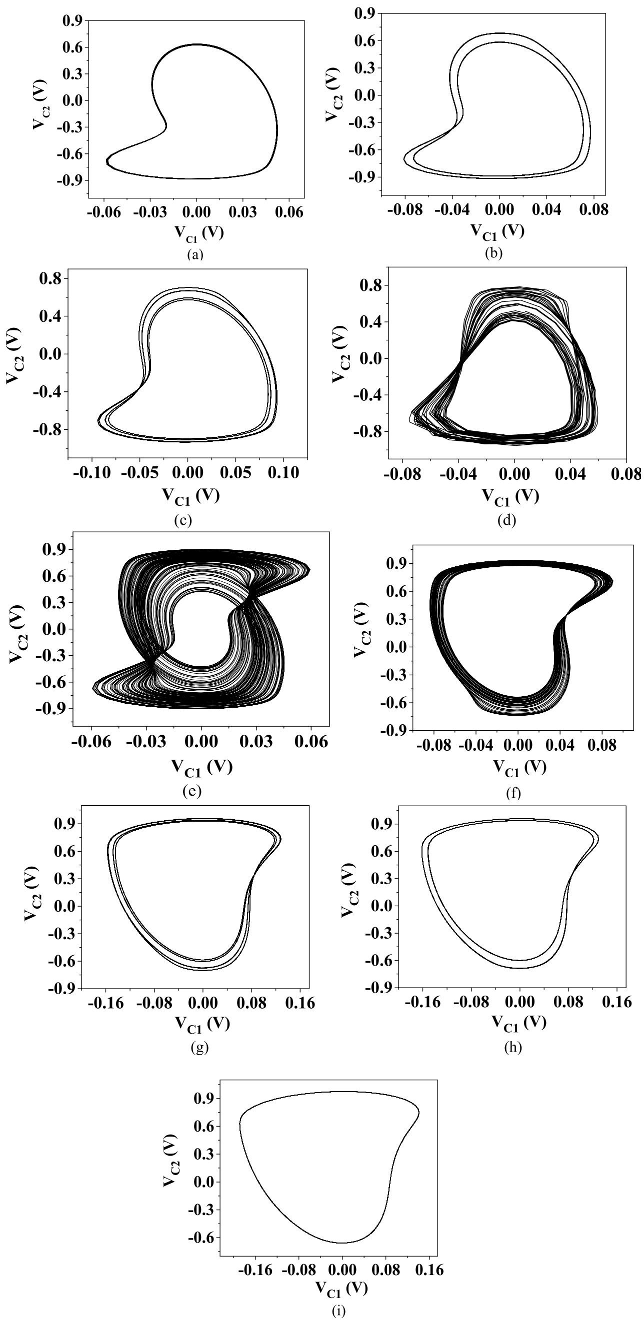

FIGURE 5. Phase portraits of V_{C1} vs. V_{C2} for; (a) single period (I_{b1}=195μA), (b) period-2 (I_{b1}=189μA), (c) period-4 (I_{b1}=184μA), (d) single scroll (I_{b1}=171μA), (e) double scroll (I_{b1}=164μA), (f) single scroll (I_{b1}=154.7μA), (g) period-4 (I_{b1}=151μA), (h) period-2 ((I_{b1}=148μA), (i) single period (I_{b1}=144μA).

parameter's space, where the oscillator develops different coexisting attractors. The coexistence of different attractors in a space domain is identified as multistability, and to investigate this, regions of coexisting attractors are traced over a range of control parameter's space with different initial conditions, (x(0), y(0), z(0)). Some advanced dynamic systems have investigated such a phenomenon [30], [31]. Multistability is a parameter-independent phenomenon in advanced chaotic systems for forming different attractors by selecting different initial conditions. In the proposed oscillator, this exciting phenomenon is investigated through circuit-level simulations with different initial conditions and control parameter 'a' (i.e., I_{b1}). In the proposed circuit-level simulation, different initial conditions are selected with different values of I_{b1}. Multiple coexisting attractors of V_{C2} vs. I_L and V_{C1} vs. I_L are obtained with fixed parameter values as $b = 50$ and $\beta = 0.8944^{*}10^{3}$. As depicted in Fig. 10-13, a set

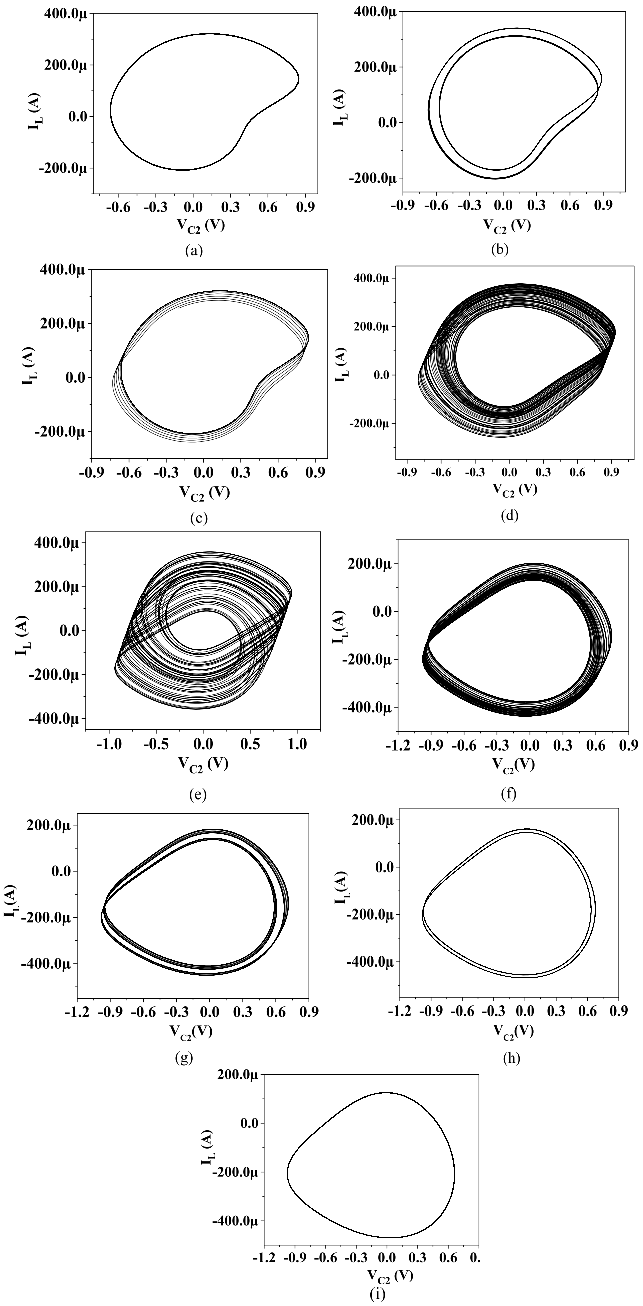

FIGURE 6. Phase portraits of V_{C2} vs. I_L for; (a) single period ($I_{b1}=195\mu A$), (b) period-2 ($I_{b1}=189\mu A$), (c) period-4 ($I_{b1}=184\mu A$), (d) single scroll ($I_{b1}=171\mu A$), (e) double scroll ($I_{b1}=164\mu A$), (f) single scroll ($I_{b1}=154.7\mu A$), (g) period-4 ($I_{b1}=151\mu A$), (h) period-2 (($I_{b1}=148\mu A$), (i) single period ($I_{b1}=144\mu A$).

of four disconnected co-existing attractors for V_{C2} vs. I_L are obtained.

Similarly, as depicted in Fig. 14 and 15, four disconnected co-existing attractors for V_{C1} vs. I_L are obtained. It can be observed that, for two initial conditions, the attractors exhibited by the system are precisely similar, except the directions of the trajectories are different. It may be noted that investigation of multistability at the circuit level with intrinsic electronic tuneability has not been found in reported chaotic oscillator designs.

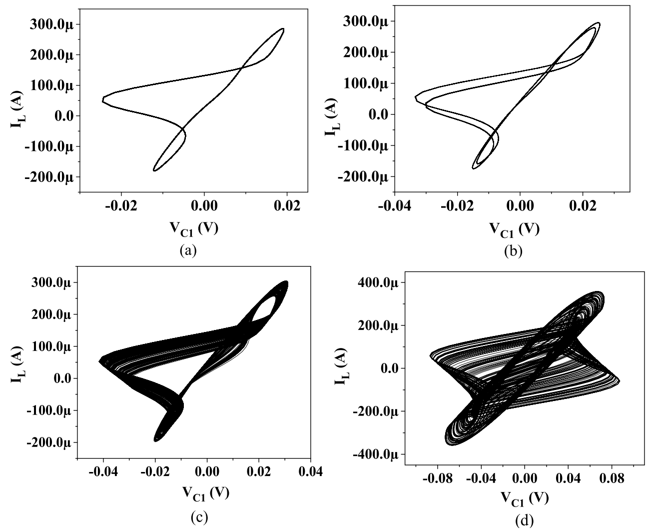

FIGURE 7. Phase portraits of V_{C1} vs. I_L for; (a) single period (($I_{b1}=195\mu A$) (b) period 2 (($I_{b1}=189\mu A$) (c) single scroll (($I_{b1}=171\mu A$) (d) double scroll ($I_{b1}=164\mu A$).

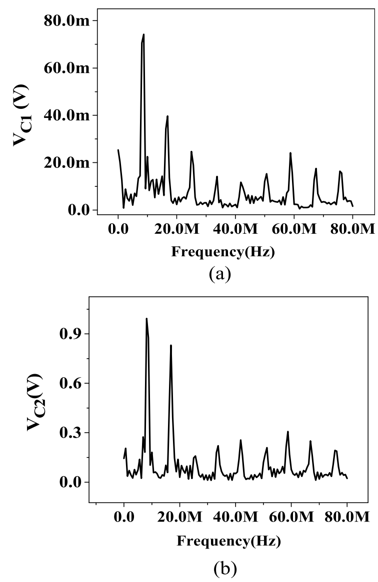

FIGURE 8. Frequency spectrum for chaotic oscillations; (a) V_{C1} (b) V_{C2}.

VI. 4D CHAOTIC OSCILLATOR

High dimensional chaotic oscillators are in enormous demand due to their potential applications in secure communication, such as cryptography and chaos synchronization [42], [43], [44], [47], [52], [53], [54], [55], [56], [57], [58]. Some 4D or hyperjerk circuits have been reported in [42], [43], [44], [47], [52], [53], [54], [55], [56], [57], and [58], exhibiting complex dynamical behaviours through phase portraits. In this section, a new four-dimensional (4D) chaotic oscillator circuit is proposed as an extension of the 3D circuit in Fig. 2. The proposed 4D chaotic oscillator is shown in Fig. 16, which results by connecting one grounded capacitor C_3 and a resistance R_O in the circuit of Fig. 2. It is a simple 4D chaotic oscillator employing minimum possible components and possessing electronic tuneability feature.

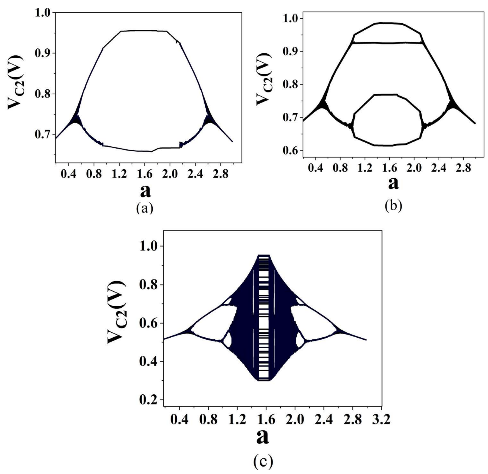

FIGURE 9. Bifurcation diagram for V_{C2} versus 'a' for (a) single period for b=0.8 (b) period-2 for b=4 (c) double scroll for b=48.

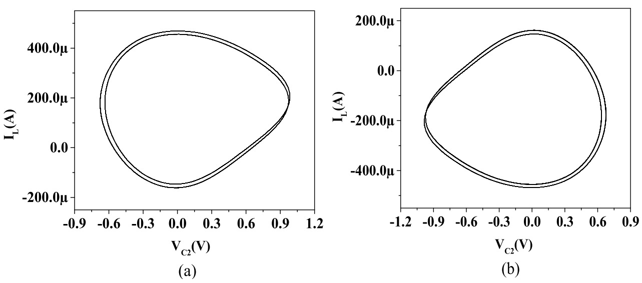

FIGURE 10. Coexistence of period-2 attractors (V_{C2} vs. I_L) for I_{b1}=186μA, and $(x(0), y(0), z(0))$ as, (a) (0, 0.8, 0) (b) (0, −0.8, 0).

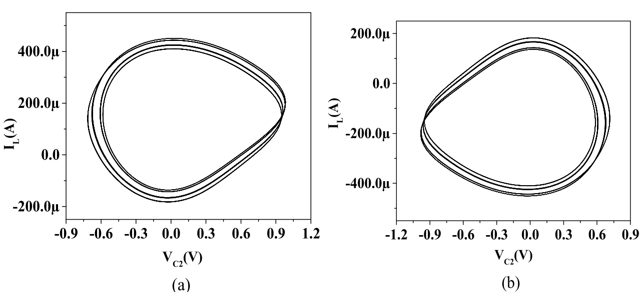

FIGURE 11. Coexistence of period-4 attractors (V_{C2} vs. I_L) for I_{b1}=186μA, and $(x(0), y(0), z(0))$ as, (a) (0, 1, 0), (b) (0, −1, 0).

Governing equations of the proposed 4D chaotic circuit, as shown in Fig. 16, are a set of four first-order differential equations as follows:

$$
\begin{aligned}
C_1\frac{dV_{C2}}{dt} &= -\frac{V_{C1}}{R_X} + I_{NL} + \frac{V_{C3}-V_{C1}}{R_o};\\
C_2\frac{dV_{C1}}{dt} &= -\frac{V_{C1}}{R_X};\\
L\frac{dI_{L1}}{dt} &= V_{C2} - V_{C3};\\
C_3\frac{dI_{L2}}{dt} &= I_L - \frac{V_{C3}-V_{C1}}{R_o};
\end{aligned} \tag{14}
$$

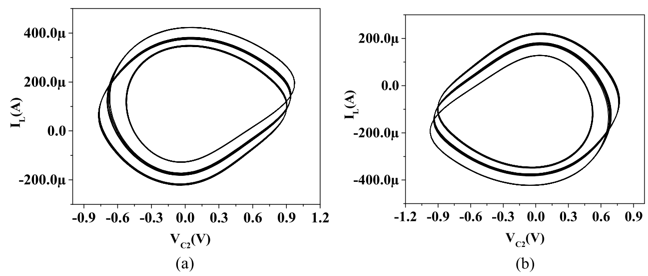

FIGURE 12. Coexistence of attractors (V_{C2} vs. I_L) for I_{b1}=174μA, and $(x(0), y(0), z(0))$ as, (a) (0, 0.8, 0) (b) (0, −0.8, 0).

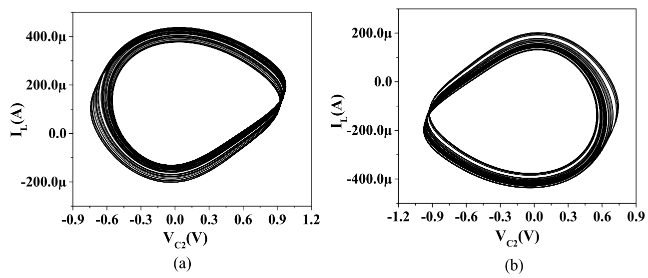

FIGURE 13. Coexistence of single scroll attractors (V_{C2} vs. I_L) for I_{b1}=174μA, and $(x(0), y(0), z(0))$ as, (a) (0, 1, 0), (b) (0, −1, 0).

On expressing model equations in dimensionless state variable form, (14) results as;

$$
\begin{aligned}
\dot{x} &= -ax + c\,(w-x) + \varphi\sinh(y-x);\\
\dot{y} &= -abx;\\
\dot{z} &= y - w;\\
\dot{w} &= \rho z - \rho c(w-x);
\end{aligned} \tag{15}
$$

where,

$$
\begin{aligned}
&x = \frac{V_{C1}}{V_r},\quad y = \frac{V_{C2}}{V_r},\ z = \frac{\beta I_{L1}}{V_r},\quad w = \frac{V_{C3}}{V_r},\\
&a = \frac{\beta}{R_X},\quad c = \frac{\beta}{R_O}\ b = \frac{C_1}{C_2},\quad \beta = \sqrt{\frac{L}{C_1}},\ \rho = \frac{C_1}{C_3},\\
&\varphi = \frac{2aI_S}{V_r},\ \text{and } t = \tau\sqrt{LC_1}
\end{aligned} \tag{16}
$$

A. DYNAMICAL ANALYSIS OF 4D CHAOTIC OSCILLATOR

1) DISSIPATIVITY

In order to verify the existence of attractors in the proposed 4D system as given in (15), divergence (∇) of volume (V) of the system (15) is taken as per (9) in line with section III, B, and it results as;

$$
\nabla V = -a - c - \rho c - \varphi\cosh(y-x) < 0 \tag{17}
$$

At any given point (x, y), the term '$-\varphi\cosh(y-x)$' will always be negative. Therefore, (17) depicts that ∇V will always be less than zero; it proves that system (15) is dissipative.

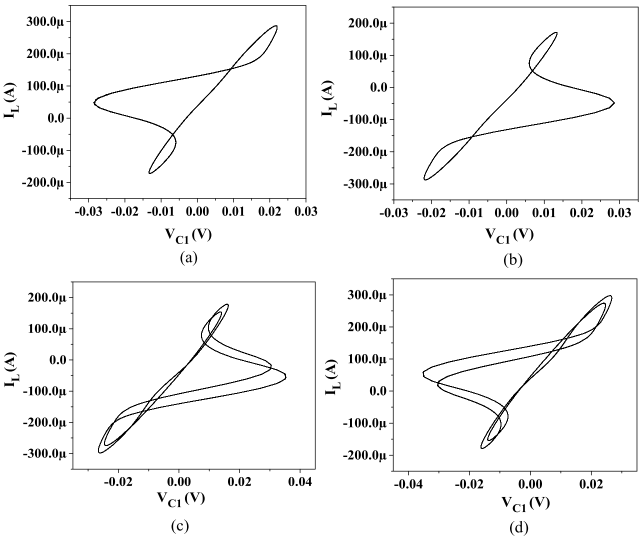

FIGURE 14. Coexistence of single periodic attractors (V_{C1} vs. I_L) for I_{b1}=186μA, with ($x(0)$, y(0), z(0)) as, (a) (.01, 0,0), (b) (−.01, 0,0); and period-2 attractors with, (c) (.04, 0,0), (d) (−.04, 0,0).

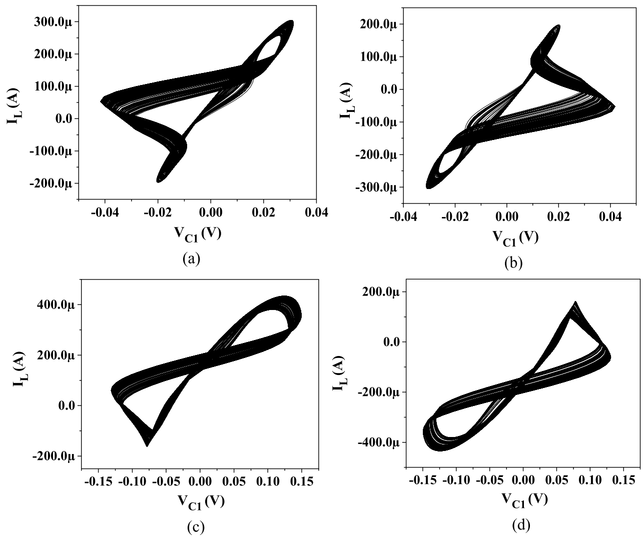

FIGURE 15. Coexistence of single scroll attractors (V_{C1} vs. I_L) for I_{b1}=174μA, with ($x(0)$, y(0), z(0)) as, (a) (.01, 0,0), (b) (−.01, 0,0), and (c) (.04, 0,0), (d) (−.04, 0,0).

2) EQUILIBRIUM POINT AND STABILITY

The equilibrium point of system (15) is the origin (0, 0, 0, 0), and eigenvalues of (15) are calculated by det $(M_J - \lambda I) = 0$, where Jacobian matrix (M_J) for (15) is obtained with a 4 × 4 identity matrix 'I' as per (11). The resulting characteristic equation is obtained as follows:

$$\lambda^4 + \lambda^3 n_3 + \lambda^2 n_2 + \lambda n_1 + n_O = 0 \tag{18}$$

where, $n_3 = \rho c + a + c + \varphi$; $n_2 = \rho ac + \varphi ab + \rho + \rho c\varphi$; $n_1 = \rho\varphi + abc\rho\varphi + a\rho + c\rho$;

$$n_O = abc\rho + \varphi\rho ab \tag{19}$$

For a case of parameter values as, (a, b, c, ρ) = (1.12, 50, 0.2236, 1), and $\varphi = 0.58{*}10^{-4}$, using (19), the eigenvalues for (18) are obtained as, $\lambda_{1,2} = -1.6802 \pm j1.2886$, $\lambda_{3,4} = 0.8966 \pm j1.4101$. The positive real part in the eigenvalue ($\lambda_{3,4}$) strongly indicates that the origin is unstable in the chaotic regime.

3) BIFURCATION AND ROUTE TO CHAOS

The bifurcation diagram showing the transition to chaos in the proposed 4D system (15) on varying bifurcation control parameter 'a' is shown in Fig. 17(a). The plot from numerical simulation in MATLAB and the plot obtained from circuit simulation's time series data in PSpice are compared in Fig. 17(a). For fixed parameters (b=50, c = 0.2236, ρ = 1), 'a' is being varied, and corresponding 'x' is obtained without resetting the initial condition. There is the development of a rich bifurcation process indicating local maxima for 'x' over a wide range of 'a'. Further, the plots for Lyapunov exponents are depicted in Fig. 17(b). The highest positive exponent corresponds to 1.58 (red color), which confirms the chaoticity in the proposed 4D circuit. It is observed that numerical simulated responses depict close agreement to responses obtained from the circuit's data.

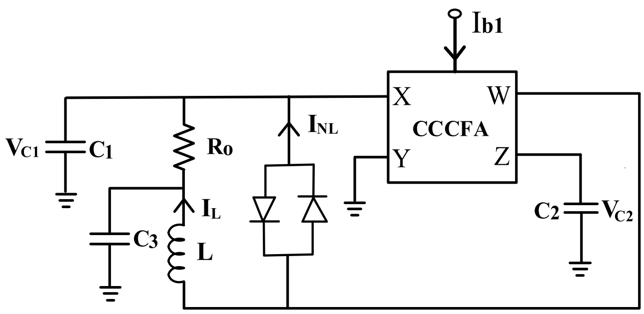

FIGURE 16. Proposed 4D chaotic oscillator circuit.

4) LYAPUNOV STABILITY DIAGRAM

Lyapunov stability diagram depicting dynamical regions with variation in two bifurcation parameters, 'a' and 'b' for the proposed 4D system, is shown in Fig. 17(c). Blue corresponds to a stable state, green to a periodic region, yellow to quasiperiodic, and red to a chaotic region. It indicates proposed 4D system possesses periodicity and chaotic behaviour over a considerable range of parameter values, and the chaotic characteristics of the proposed system are more complex and difficult to predict. Fig. 17(c) also depicts the Lyapunov exponents corresponding to chaotic and periodic regions.

B. SIMULATION RESULTS FOR 4D CHAOTIC OSCILLATOR

The complex attractors of different varieties are obtained for 4D topology of Fig. 16, for C_1 = 50pF, C_2 = 1pF, L=40μH, C_3 = 50pF, and R_O = 4kΩ as depicted in Fig. 18-25. Complex structures of phase portraits are characteristics of a higher dimensional chaotic system, as the simulated attractors exhibit. 4D double scroll attractors corresponding to the phase portrait of V_{C1} vs. V_{C3} are shown in Fig. 18(a) and (b) for I_{b1} = 195μA and I_{b1} = 166.7μA, respectively. Double scroll attractors corresponding to V_{C3} vs. V_{C2} are shown in Fig. 19(a) and (b), whereas

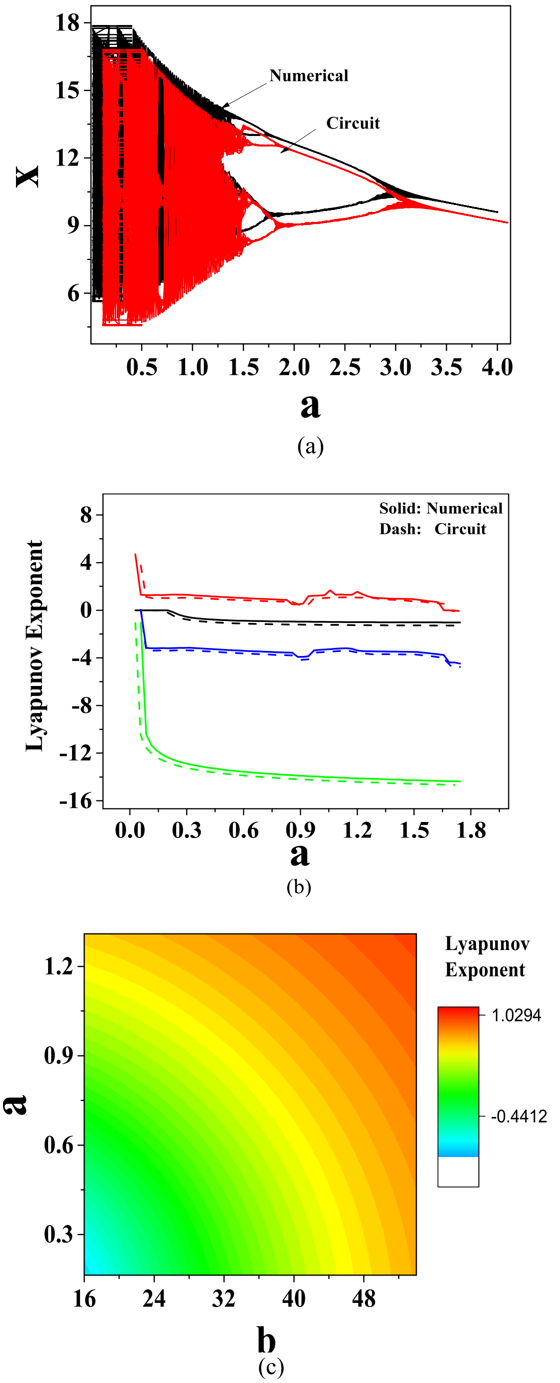

FIGURE 17. Plots for (a) bifurcation diagram, (b) Lyapunov exponents, (c) Lyapunov stability diagram for 'a' vs. 'b'.

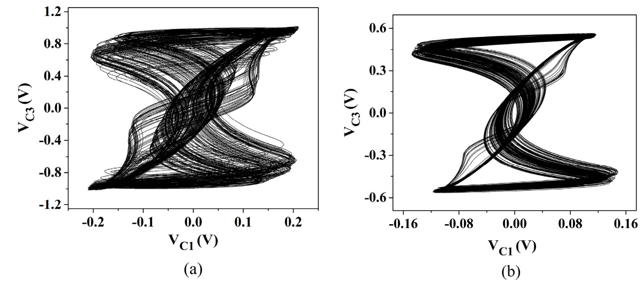

FIGURE 18. 4D double scroll attractors of V_{C1} vs. V_{C3} for (a) I_{b1}=195μA, (b) I_{b1}=166.7μA.

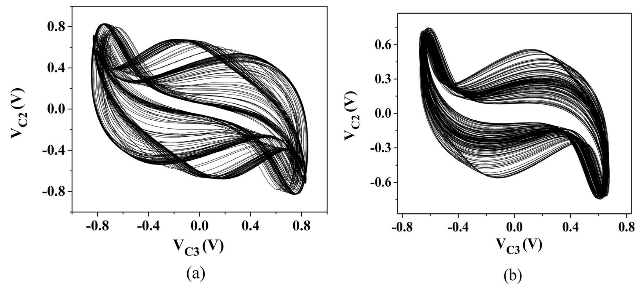

FIGURE 19. 4D double scroll attractors of V_{C3} vs. V_{C2} for (a) I_{b1}=195μA, (b) I_{b1}=166.7μA.

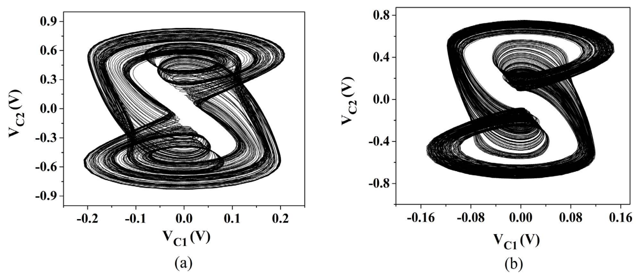

FIGURE 20. 4D double scroll attractors of V_{C1} vs. V_{C2} for (a) I_{b1}=195μA, (b) I_{b1}=166.7μA.

corresponding to V_{C1} vs. V_{C2} are shown in Fig. 20(a) and (b). Further, to observe periodicity and route to chaos, various periodic and single scroll attractors corresponding to V_{C1} vs. V_{C3}, V_{C2} vs. V_{C3}, and V_{C1} vs. V_{C2} are obtained as shown in Fig. 21(a)-(d), 22(a)-(d) and 23(a)-(d) respectively. Moreover, phase portraits of I_L vs. V_{C1} and I_L vs. V_{C2} depicting periodic, single scroll, and double scroll attractors are shown in Fig. 24(a)-(e) and 25(a)-(e), respectively. It is observed from Fig. 18-25 that the proposed 4D circuit develops a wide variety of complex attractors in all the planes. It may also be noted that the phenomenon of forming various complex attractors in all the planes through electronic tuneability in a 4D chaotic oscillator is not reported in the available literature.

C. MULTISTABILITY IN 4D CHAOTIC OSCILLATOR

Multistability is investigated in the proposed 4D chaotic oscillator circuit in Fig. 16 to illustrate the phenomenon of the coexistence of attractors. Circuit level investigation is done on selecting different set of initial conditions, (x(0), y(0), z(0), w(0)) and tuning of I_{b1} (i.e. control parameter 'a'). Various sets of disconnected coexisting attractors are obtained for different initial conditions and I_{b1}, as depicted in Fig. 26-29. It may be noted that circuit-level investigation of multistability in 4D chaotic oscillators through electronic tuneability is not reported in any available literature.

VII. APPLICATION IN CHAOS ENCRYPTION

In the communication system, there is a necessity for the secure transmission of the information signal, which

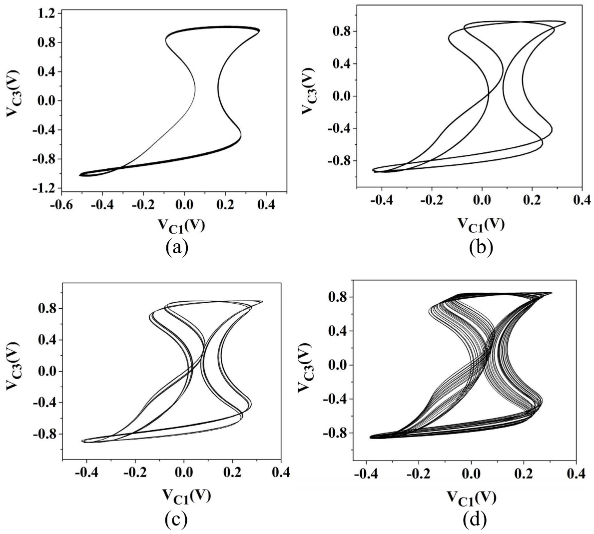

FIGURE 21. Phase portraits of V_{C1} vs. V_{C3} for (a) single period (I_{b1}=144μA), (b) period-2 (I_{b1}=148μA), (c) period-4 (I_{b1}=151μA), (d) single scroll (I_{b1}=154.7μA) attractors.

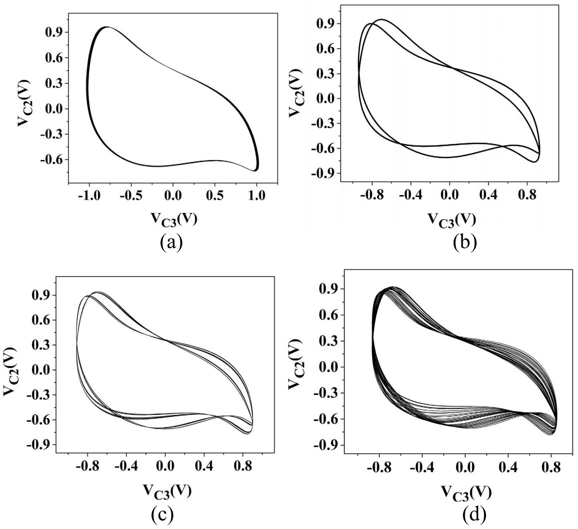

FIGURE 22. Phase portraits of V_{C3} vs. V_{C2} for; (a) single period (I_{b1}=144μA), (b) period-2 (I_{b1}=148μA), (c) period-4 (I_{b1}=151μA), (d) single scroll (I_{b1}=154.7μA) attractors.

raises the need for many cryptographic techniques. One of the most employed techniques is chaos encryption, which uses a chaotic signal as a carrier signal. High dimensional (4D) chaotic systems find wide application in these techniques over the 3D system due to their complex dynamical behaviour. Here the proposed 3D and 4D chaotic oscillators are demonstrated as an application in the encryption of electrocardiogram signal (ECG), as illustrated in Fig. 30. In this technique, chaotic (V_{C2}) and ECG (V_G) signals are added and then multiplexed with V_{C2} [65]. This encrypted signal is transmitted over the channel and demultiplexed at the receiver. After this, the result gets subtracted, and the decrypted ECG signal is obtained through a low pass filter (LPF). Adder and subtractor circuits are shown

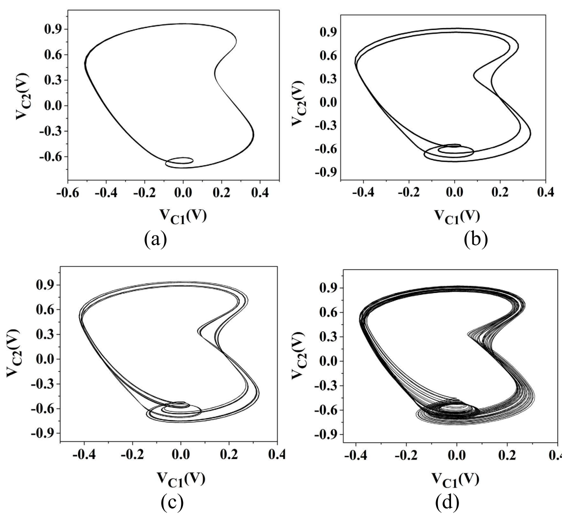

FIGURE 23. Phase portraits of V_{C1} vs. V_{C2} for (a) single period (I_{b1}=144μA), (b) period-2 (I_{b1}=148μA), (c) period-4 (I_{b1}=151μA), (d) single scroll (I_{b1}=154.7μA) attractors.

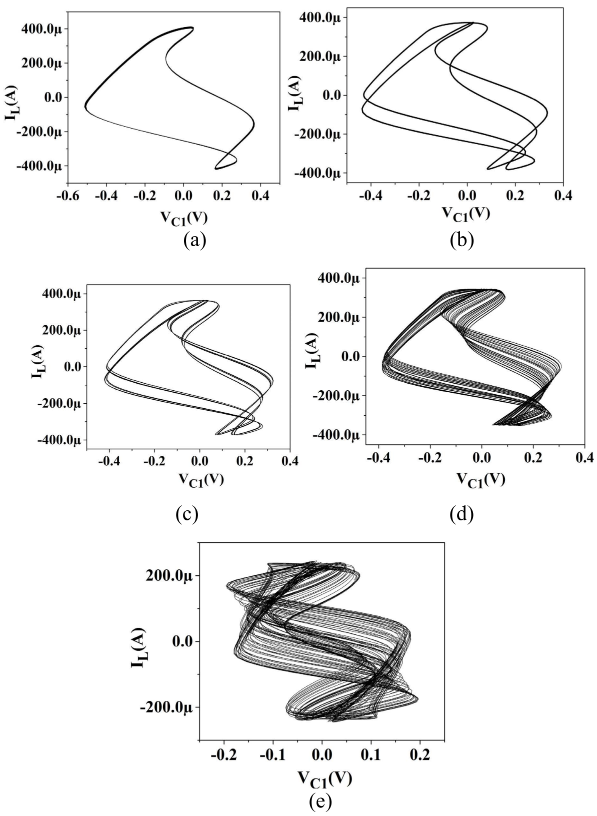

FIGURE 24. Phase portraits of V_{C1} vs. I_L for; (a) single period (I_{b1}=144μA), (b) period-2 (I_{b1}=148μA), (c) period-4 (I_{b1}=151μA), (d) single scroll (I_{b1}=154.7μA) (e) double scroll (I_{b1}=164μA) attractors.

in Fig. 31(a) and (b). IC ADG659 implements multiplexer (MUX) and demultiplexer (DE-MUX), while LPF is a simple RC circuit. In this technique, the information signal is actually deducted from the transmitted signal instead of the estimation [65], however, for secure transmission of signal, the attacker should not have the DE-MUX with same select

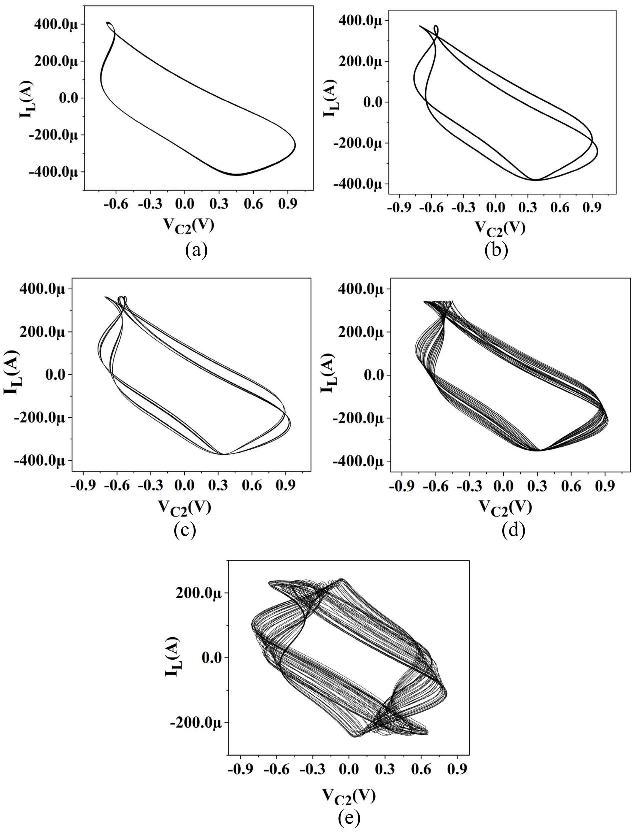

FIGURE 25. Phase portraits of V_{C2} vs. I_L for; (a) single period ($I_{b1}=144\mu A$), (b) period-2 ($I_{b1}=148\mu A$), (c) period-4 ($I_{b1}=151\mu A$), (d) single scroll ($I_{b1}=154.7\mu A$) (e) double scroll ($I_{b1}=164\mu A$) attractors.

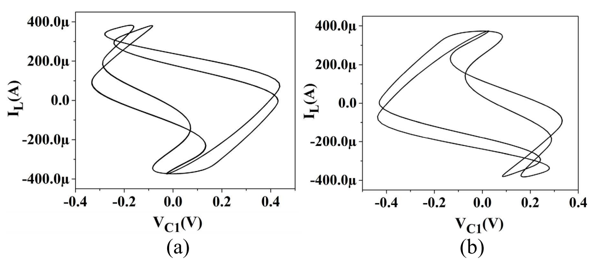

FIGURE 26. Coexistence of period-2 attractors (V_{C1} vs. I_L) for $I_{b1}=148\mu A$ and ($x(0)$, $y(0)$, $z(0)$, $w(0)$) as, (a) (0.2, 0, 0, 0) (b) (−0.2, 0, 0, 0).

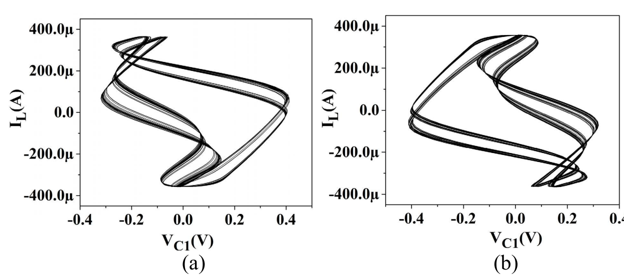

FIGURE 27. Coexistence of quasi-periodic attractors (V_{C1} vs. I_L) for $I_{b1}=148\mu A$ and ($x(0)$, $y(0)$, $z(0)$, $w(0)$) as, (a) (0.4, 0, 0, 0) (b) (−0.4, 0, 0, 0).

line pulse signal as of the receiver. The simulated waveforms for 3D and 4D chaotic oscillators are shown in Fig. 32 and 33, respectively. It is observed that the encrypted signal, as shown

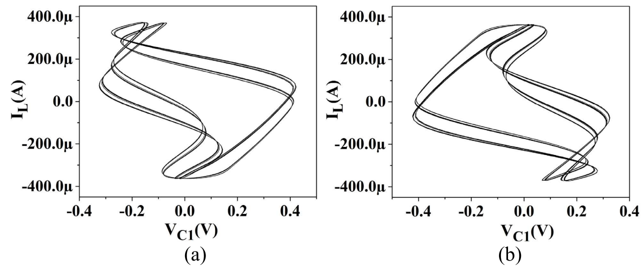

FIGURE 28. Coexistence of period-4 attractors (V_{C1} vs. I_L) for $I_{b1}=154\mu A$ and ($x(0)$, $y(0)$, $z(0)$, $w(0)$) as, (a) (0.2, 0, 0, 0) (b) (−0.2, 0, 0, 0).

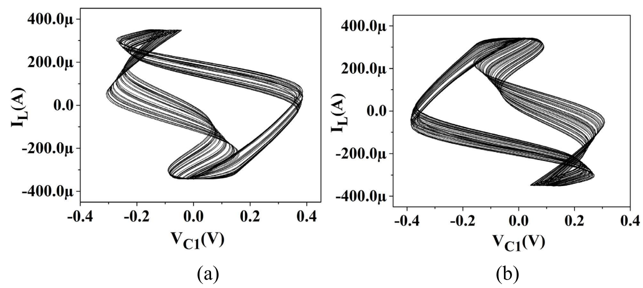

FIGURE 29. Coexistence of single scroll attractors (V_{C1} vs. I_L) for $I_{b1}=154\mu A$ and ($x(0)$, $y(0)$, $z(0)$, $w(0)$) as, (a) (0.4, 0, 0, 0) (b) (−0.4, 0, 0, 0).

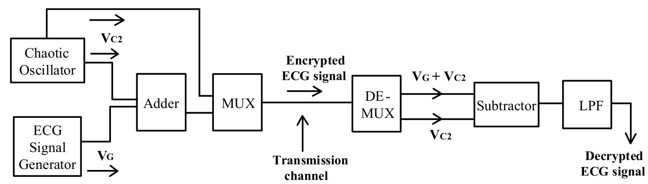

FIGURE 30. Chaos encryption scheme of ECG signal using a chaotic oscillator.

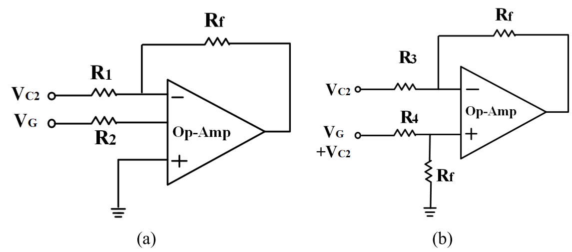

FIGURE 31. Op-amp based circuits for; (a) adder (b) subtractor.

in Fig. 33(b) for a 4D chaotic oscillator, depicts a higher degree of chaos and complexity as compared to 3D, shown in Fig. 32(c). This verifies the complex and unpredictable chaotic behaviour of the proposed 4D chaotic circuit and assures the application of the proposed oscillator in the secure transmission of the information signal in communication systems.

VIII. EXPERIMENTAL RESULTS

The proposed chaotic oscillator using commercially available IC, AD844, is shown in Fig. 34 for experimental verification. The CCCFA is implemented with one AD844 and resistance, R_1 in place of intrinsic resistance, R_X at the X terminal of CCCFA. The supply voltage is set as ±5V, with selected values of components, $C_1 = 50$ pF, $C_2 = 1$pF, and $L = 40\mu$H.

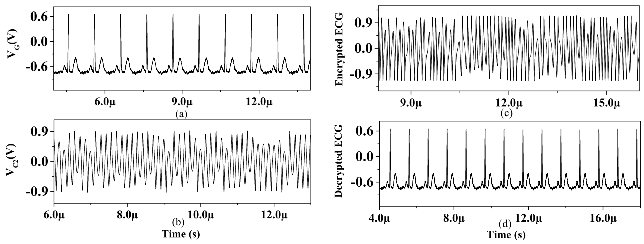

FIGURE 32. Encryption with 3D chaotic oscillator; (a) ECG signal (b) chaotic signal (c) encrypted ECG signal (d) decrypted ECG signal.

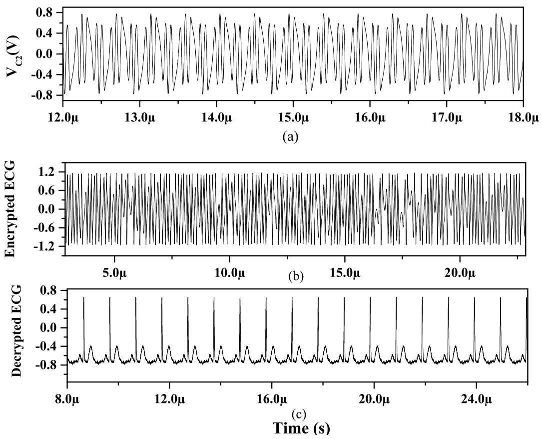

FIGURE 33. Encryption with 4D chaotic oscillator; (a) chaotic signal (b) encrypted ECG signal (c) decrypted ECG signal.

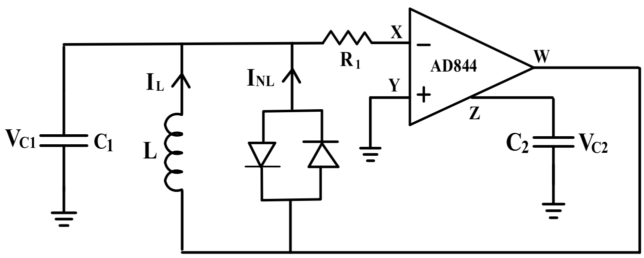

FIGURE 34. Implementation of the proposed chaotic circuit using AD844.

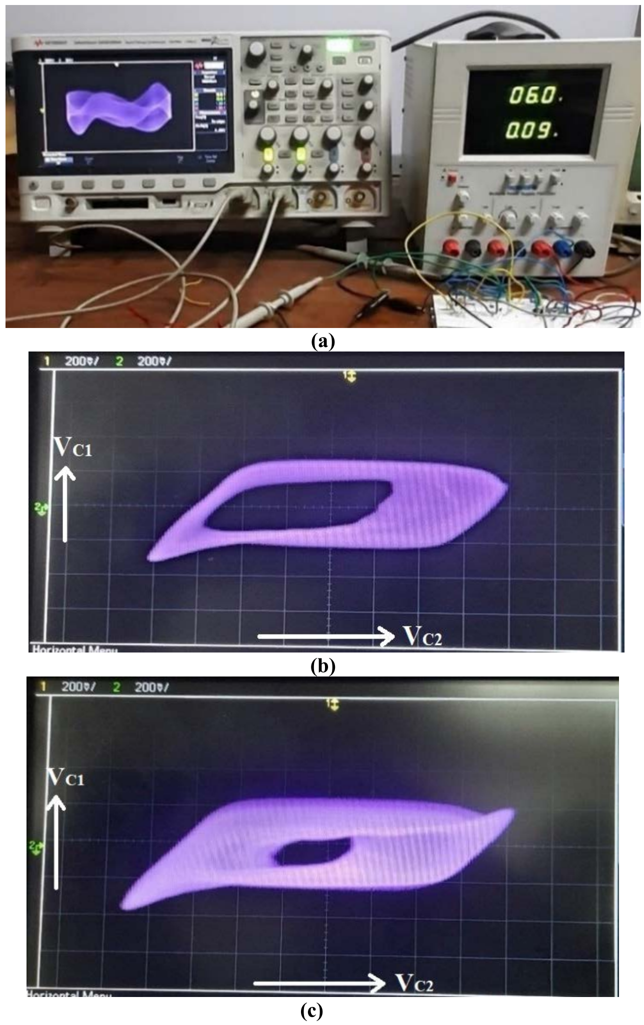

FIGURE 35. Experimental; (a) set up, (b) single scroll attractor (V_{C2} vs. V_{C1}) for 3D, (c) double scroll attractor (V_{C2} vs. V_{C1}) for 3D.

Fig. 35(a) shows the experimental setup. The response of the single scroll attractor of the 3D circuit is shown in Fig. 35(b) for $R_1 = 300\Omega$, whereas the double scroll attractor is shown in Fig. 35(c), obtained at $R_1 = 440\Omega$. Moreover, various double scroll attractors of the proposed 4D circuit are shown in Fig. 36(a)-(c). Double scroll attractors corresponding to V_{C1} vs. V_{C3} and V_{C2} vs. V_{C3} are shown in Fig. 36(a) and (b), respectively, for $R_1 = 480\Omega$. Double scroll attractor of V_{C1} vs. V_L is shown in Fig. 36(c), where V_L corresponds to the voltage across L. Parameter values for the 4D circuit are set as; $C_3 = 50$pF, $R_O = 8$kΩ as per circuit of Fig. 16.

IX. COMPARISON WITH THE AVAILABLE LITERATURE

The comparison of the reported literature is given in Table 2. It is observed that designs [4, 8, 9 (Fig. 1(b, c)), 11, 13 (Fig. 6a), 20-26, 46] use 2-12 ABBs, and designs [9 (Fig.2b), 10, 12, 13 (Fig. 2a), 14-18, 22, 39-41, 45] employ only one ABB as that of the proposed work. The number of passive components in the count is excessive in [4], [8], [9], [10], [11], [12], [13], [14], [15], [19], [20], [21], [22], [23], [24], [25], [26], [28], [29], and [40]. The possession of smooth symmetrical nonlinearity is desirable for rich chaotic responses, and the topologies [13 (Fig. 6a), 23, 25, 26, 39-41, 45, 46] possess this property. The electronic tuning feature is available in [16] and [24], whereas the formation of attractors through electronic tuning is not available in [24]. Transistor-based chaotic oscillators [32], [34], [35] possess many shortcomings. The circuit in [32] has shortcomings as an excessive number of resistors in the circuit, low operating frequency, and asymmetry in upper and lower bands of double scroll attractors (i.e., not exactly symmetric nonlinearity). Moreover, [32] does not exhibit advanced dynamical phenomena of multistability. Designs in [34] and [35] have an absence of symmetric nonlinearity, hence cannot generate the double scroll attractors and are not able to exhibit advanced dynamical phenomena, e.g., multistability. Moreover, [32], [34], [35] have not extended the designs to 4D circuits to obtain complex attractors. Advanced dynamical phenomena

TABLE 2. Comparison of proposed 3D and 4D chaotic oscillators with available literature.

Ref.	No. and type of Analog Building Blocks (ABB) /FETs/ Diodes	No. of Passive elements	Presence of smooth symmetric nonlinearity	Availability of Bifurcations through control parameter (R)	Electronic Tuning feature	Advanced Dynamical phenomena with investigation of Multistability	No. of ICs used for practical realization	Dominant Operating Frequency (Hz)	Extended to new 4D chaotic oscillator with electronic tuneability	Multistability and complex attractors in all the planes in 4D chaotic oscillator
[4]	2 Op-Amp	2C, 1L,7R	No	Yes	No	No	2	NA	No	No
[8]	3 Op-Amp	3C, 10R	No	Yes	No	No	3	NA	No	No
[9]	Fig. 1(b),(c): 2 VOAs/ CFOAs	2C, 1L, 4-6R	No	Yes	No	No	2	NA	No	No
	Fig. 2(b): 1 CFOA 1 JFET	3C, 5R	No	Yes	No	No	1	20.5k	No	No
[10]	1 Op- Amp 1 JFET	3C, 3R	No	Yes	No	No	1	NA	No	No
[11]	Fig. 3, 4: 2 VOAs, 1 CFOA	3C, 11R	No	Yes	No	No	3	NA	No	No
	Fig. 5, 6, 15: 2 VOAs / 1-2 CFOAs, 1 Diode	2-3C, 1L, 4-8R	No	Yes	No	No	2, 1	NA	No	No
	Fig. 11, 13: 1 VOA / 2 CFOAs 1 JFET	3C, 4R	No	Yes	No	No	1	NA	No	No
[12]	1 CFOA, 1 JFET	2C, 1L, 3R	No	Yes	No	No	1	1.35M	No	No
[13]	Fig. 2a : 1 Op-Amp, 1 JFET	3C, 3-4 R	No	Yes	No	No	1	0.58M	No	No
	Fig. 6a : 2 Op-Amp, 2 Diodes	3C, 8R	Yes	Yes	No	No	2	NA	No	No
[14]	1 CCII 1 JFET	3C, 3R	No	Yes	No	No	1	NA	No	No
[15]	1 Op-Amp 1 Diode	2C, 1L, 4R	No	Yes	No	No	1	58k	No	No
[16]	1 Op-Amp 1 Diode	2C, 1L	No	Yes	Yes	No	1	NA	No	No
[17]	1 Op-Amp 1 Diode	2C, 1L, 1R	No	Yes	No	No	1	NA	No	No
[18]	1 Op-Amp 1 JFET	2C, 1L, 1R	No	Yes	No	No	1	NA	No	No
[19]	2 CFOAs	2C, 1L, 5R	No	Yes	No	No	2	522k	No	No
[20]	4 MOCCII	3C, 7R	No	Yes	No	No	NA	NA	No	No
[21]	3 DVCCTA	3C, 6R	No	Yes	No	No	12	NA	No	No
[22]	1 VDTA	2C, 1L,2R	No	Yes	No	No	2	10M	No	No
[23]	1 Multiplier, 11 Op-Amps	3C, 24R	Yes	Yes	No	NA	12	5k	No	No
[24]	Fig. 3,4,5,6 : Multiplier, 3-7 OTAs, 1-5 VFA, 1 buffer	3C, 1-26 R	No	No	Yes	No	6 -10	Few kHz	No	No
[25]	Fig. 6, 7: 3 Multiplier, 4 Op-Amp, 9 CCII	3C, 6-8R	Yes	Yes	No	No	7,12	1M	No	No

TABLE 2. ***(Continued.)*** **Comparison of proposed 3D and 4D chaotic oscillators with available literature.**

[26]	2-Multipliers 1 Op-Amp	2C, 1L, 7R	Yes	Yes	No	No	3	Few kHz	No	No
[27]	Differential pair	2C, 1L, 1R	No	Yes	No	No	NA	1.5M	No	No
[28]	2 Inverters	2C, 1L,2R	No	Yes	No	No	NA	1 M	No	No
[29]	2 Inverters	2C,1L,3R	No	Yes	No	No	NA	1 M	No	No
[32]	2 Transistors	4C, 7R	*No	Yes	No	No	NA	kHz	No	No
[34]	1 Transistor	2 L,	No	No	Yes	No	NA	NA	No	No
[35]	1 Transistor	2C,1L, 2R	No	Yes	Yes	No	NA	NA	No	No
[39]	1 CFOA, 2 Diodes	2C, 1L, 1R	Yes	No	No	No	1	NA	No	No
[40]	1 OpAmp, 2 Diodes	2C, 1L, 3R	Yes	Yes	No	No	1	NA	No	No
[41]	1 OpAmp, 2 Diodes	2C, 1L, 1R	Yes	Yes	No	Yes	1	NA	No	No
[45]	1 OTRA, 2 Diodes	2C, 1L, 2R	Yes	Yes	No	No	2	7.8M	*Yes	No
[46]	1 CFOA, 1 Inverter, 2 Diodes	2C, 1L, 1R	Yes	No	No	No	2	NA	*Yes	No
This Work	1 CCCFA 2 Diodes	2C, 1L	Yes	Yes	Yes	Yes	1	8.4M	Yes	Yes

Note: *Yes: Tuning is not through intrinsic resistance of ABB; *No: Not exactly symmetric.

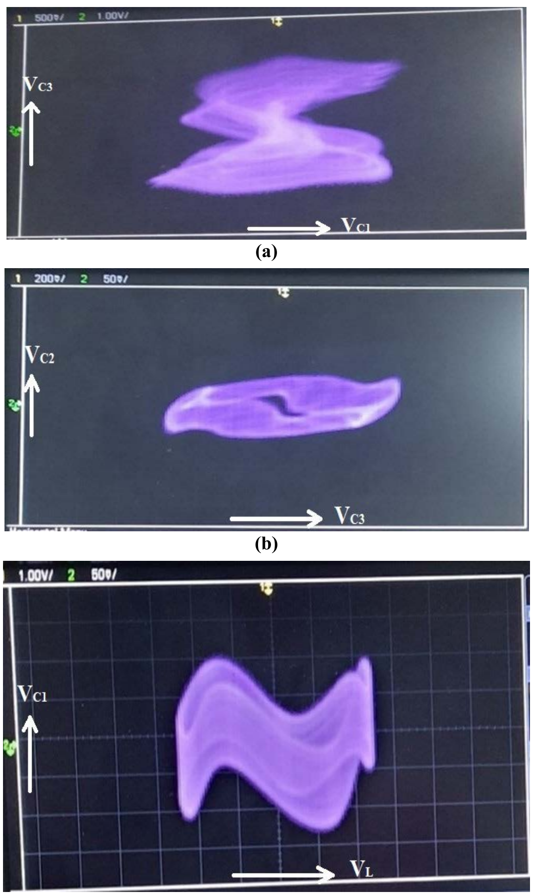

FIGURE 36. **Double scroll attractors of 4D circuit; (a) V_{C1} vs. V_{C3} (b) V_{C3} vs. V_{C2} (c) V_L vs. V_{C1}.**

of multistability/coexisting attractors are reported only in [41]. Topologies [39], [40], [45] employ one ABB and possess smooth symmetrical nonlinearity, however, [39] is controllable through L and does not have bifurcation parameter R, [40] uses excessive resistors and [45] use 2R and two ICs for practical implementation. In [46], the formation of different attractors is through variation in C and L, which is not desirable; moreover, electronic tuneability is not possible, and the advanced multistability phenomenon has also not been investigated. Further, it may also be noted that two active blocks are used to implement a chaotic circuit in [46]. The proposed chaotic oscillator uses minimum active and passive components, employing only one ABB, two Cs, and one L. It is resistorless and possesses smooth symmetric nonlinearity. The circuit is electronically tuneable through intrinsic resistance of ABB and presents the circuit-level investigation of the advanced chaotic phenomenon of multistability. Moreover, the dominant operating frequency of chaotic oscillations, as depicted in Fig. 8(a) and (b), is the highest among all the earlier available chaotic oscillators designed with smooth symmetric nonlinearity. Furthermore, a new electronically tuneable 4D chaotic oscillator is proposed by simple extension of 3D topology employing minimum active/passive components. The proposed 4D circuit develops various periodic and complex chaotic attractors in all the planes with an exhibition of coexisting attractors (i.e., the phenomenon of multistability), whereas 4D circuits in [45] and [46] neither exhibited various complex attractors in all the planes nor the multistability has been investigated and use more number of components. The proposed circuit is useful in the frequency range of 18 kHz to 16.8 MHz range.

X. CONCLUSION

This work presents a new electronically tuneable third-order autonomous chaotic oscillator using a single CCCFA. The presence of an electronically tuneable bifurcation parameter (R_X) in the circuit results in an exciting variety of periodic and chaotic attractors and bifurcations. It generates chaos with rich dynamical behaviours such as antimonotonicity and the coexistence of attractors. Further, a new 4D chaotic oscillator is obtained by Extension of 3D topology. It exhibits rich chaotic behaviour. The chaos encryption technique for secure communication presents an application of both 3D and the 4D chaotic oscillator. The proposed electronically tuneable 3D and 4D chaotic oscillators are simple circuits employing minimum possible active and passive components with smooth symmetric nonlinearity and exhibit circuit-level investigation of the advanced dynamical phenomenon of multistability. The oscillator exhibits a high dominant operating frequency. Experimental results are presented to verify the proposed chaotic oscillators' simulation results and workability.

REFERENCES

[1] S. Hayes, C. Grebogi, and E. Ott, "Communicating with chaos," *Phys. Rev. Lett.*, vol. 70, no. 20, p. 3031, 1993.

[2] M. Z. De la Hoz, L. Acho, and Y. Vidal, "A modified Chua chaotic oscillator and its application to secure communications," *Appl. Math. Comput.*, vol. 247, pp. 712–722, Nov. 2014.

[3] L. O. Chua, C. W. Wu, A. Huang, and G.-Q. Zhong, "A universal circuit for studying and generating chaos. I. Routes to chaos," *IEEE Trans. Circuits Syst. I, Fundam. Theory Appl.*, vol. 40, no. 10, pp. 732–744, Oct. 1993.

[4] M. P. Kennedy, "Robust OP amp realization of Chua's circuit," *Frequenz*, vol. 46, nos. 3–4, pp. 66–80, Jan. 1992.

[5] J. R. Piper and J. C. Sprott, "Simple autonomous chaotic circuits," *IEEE Trans. Circuits Syst. II, Exp. Briefs*, vol. 57, no. 9, pp. 730–734, Sep. 2010.

[6] J. C. Sprott, "A new chaotic jerk circuit," *IEEE Trans. Circuits Syst. II, Exp. Briefs*, vol. 58, no. 4, pp. 240–243, Apr. 2011.

[7] E. Freire, L. Franquelo, and J. Aracil, "Periodicity and chaos in an autonomous electronic system," *IEEE Trans. Circuits Syst.*, vol. CS-31, no. 3, pp. 237–247, Mar. 1984.

[8] O. Morgul, "Inductorless realisation of Chua oscillator," *Electron. Letters.*, vol. 31, no. 17, pp. 1403–1404, 1995.

[9] A. S. Elwakil and M. P. Kennedy, "Chua's circuit decomposition: A systematic design approach for chaotic oscillators," *J. Franklin Inst.*, vol. 337, nos. 2–3, pp. 251–265, Mar. 2000.

[10] A. S. Elwakil and A. M. Soliman, "A family of Wien type oscillators modified for chaos," *Int. J. Circuit Theory Appl.*, vol. 25, no. 6, pp. 561–579, Nov. 1997.

[11] R. Kiliç and F. Yildirim, "A survey of Wien bridge-based chaotic oscillators: Design and experimental issues," *Chaos, Solitons Fractals*, vol. 38, no. 5, pp. 1394–1410, Dec. 2008.

[12] A. S. Elwakil and M. P. Kennedy, "A family of Colpitts-like chaotic oscillators," *J. Franklin Inst.*, vol. 336, no. 4, pp. 687–700, May 1999.

[13] A. S. Elwakil and A. M. Soliman, "Two modified for chaos negative impedance converter op-amp oscillators with symmetrical and antisymmetrical nonlinearities," *Int. J. Bifurcation Chaos*, vol. 8, no. 6, pp. 1335–1346, Jun. 1998.

[14] A. S. Elwakil and A. M. Soliman, "Current conveyor chaos generators," *IEEE Trans. Circuits Syst. I, Fundam. Theory Appl.*, vol. 46, no. 3, pp. 393–398, Mar. 1999.

[15] T. Banerjee, B. Karmakar, and B. C. Sarkar, "Chaotic electronic oscillator from single amplifier biquad," *AEU-Int. J. Electron. Commun.*, vol. 66, no. 7, pp. 593–597, Jul. 2012.

[16] B. Srisuchinwong and B. Munmuangsaen, "Four current-tunable chaotic oscillators in set of two diode-reversible pairs," *Electron. Lett.*, vol. 48, no. 17, pp. 1051–1053, Aug. 2012.

[17] W. San-Um, B. Suksiri, and P. Ketthong, "A simple RLCC-diode-opamp chaotic oscillator," *Int. J. Bifurcation Chaos*, vol. 24, no. 12, Dec. 2014, Art. no. 1450155.

[18] R. Tchitnga, T. Nguazon, P. H. Fotso, and J. A. Gallas, "Chaos in a single op-amp-based jerk circuit: Experiments and simulations," *IEEE Trans. Circuits Syst. II, Exp. Briefs*, vol. 63, no. 3, pp. 239–243, Mar. 2015.

[19] A. S. Elwakil and M. P. Kennedy, "Improved implementation of Chua's chaotic oscillator using current feedback op amp," *IEEE Trans. Circuits Syst. I, Fundam. Theory Appl.*, vol. 47, no. 1, pp. 76–79, Jan. 2000.

[20] G. Gandhi, "An improved Chua's circuit and its use in hyperchaotic circuits," *Anal. Integr. Circuits Signal Process.*, vol. 46, pp. 173–178, Feb. 2006.

[21] A. K. Kushwaha and S. K. Paul, "Inductorless realization of Chua's oscillator using DVCCTA," *Anal. Integr. Circuits Signal Process.*, vol. 88, no. 1, pp. 137–150, Jul. 2016.

[22] C. K. Choubey and S. K. Paul, "Implementation of chaotic oscillator by designing a simple Chua's diode using a single VDTA," *AEU-Int. J. Electron. Commun.*, vol. 124, Sep. 2020, Art. no. 153360.

[23] J. Petržela and V. Pospíšil, "Nonlinear resistor with polynomial AV characteristics and its application in chaotic oscillator," *Radioengineering*, vol. 13, no. 2, pp. 20–25, 2004.

[24] J. Petrzela, R. Stoner, and J. Slezak, "Electronically adjustable mixed-mode implementations of the jerk functions," *Contemp. Eng. Sci.*, vol. 2, pp. 441–449, Jan. 2009.

[25] J. Petržela and T. Gotthans, "New chaotic dynamical system with a conic-shaped equilibrium located on the plane structure," *Appl. Sci.*, vol. 7, no. 10, p. 976, 2017.

[26] G. Q. Zhong, "Implementation of Chua's circuit with cubic nonlinearity," *IEEE Trans. Circuits Syst. I, Fundam. Theory Appl.*, vol. 41, no. 12, pp. 934–941, Dec. 1994.

[27] A. M. Eltawil and A. S. Elwakil, "Low-voltage chaotic oscillator with an approximate cubic nonlinearity," *AEU-Int. J. Electron. Commun.*, vol. 53, no. 3, pp. 11–17, Jan. 1999.

[28] K. O'Donoghue, M. P. Kennedy, P. Forbes, M. Quand, and S. Jones, "A fast and simple implementation of Chua's oscillator using cubic like nonlinearity," *Int. J. Bifurcation Chaos*, vol. 15, no. 9, pp. 2950–2971, Sep. 2005.

[29] D. Ginestar, E. Parrilla, J. L. Hueso, and J. Riera, "Simulation of a cubic-like Chua's oscillator with variable characteristic," *Math. Comput. Model.*, vol. 52, nos. 7–8, pp. 1211–1218, Oct. 2010.

[30] G. D. Leutcho and J. Kengne, "A unique chaotic snap system with a smoothly adjustable symmetry and nonlinearity: Chaos, offset-boosting, antimonotonicity, and coexisting multiple attractors," *Chaos, Solitons Fractals*, vol. 113, pp. 275–293, Aug. 2018.

[31] A. Bayani, K. Rajagopal, A. J. Khalaf, S. Jafari, G. D. Leutcho, and J. Kengne, "Dynamical analysis of a new multistable chaotic system with hidden attractor: Antimonotonicity, coexisting multiple attractors, and offset boosting," *Phys. Lett. A*, vol. 383, no. 13, pp. 1450–1456, Apr. 2019.

[32] L. Keuninckx, G. Van der Sande, and J. Danckaert, "Simple two-transistor single-supply resistor-capacitor chaotic oscillator," *IEEE Trans. Circuits Syst. II, Exp. Briefs*, vol. 62, no. 9, pp. 891–895, Sep. 2015.

[33] E. Lindberg, K. Murali, and A. Tamasevicius, "The smallest transistor-based nonautonomous chaotic circuit," *IEEE Trans. Circuits Syst. II, Exp. Briefs*, vol. 52, no. 10, pp. 661–664, Oct. 2005.

[34] R. Tchitnga, H. B. Fotsin, B. Nana, P. H. Fotso, and P. Woafo, "Hartley's oscillator: The simplest chaotic two-component circuit," *Chaos, Solitons Fractals*, vol. 45, no. 3, pp. 306–313, Mar. 2012.

[35] M. P. Kennedy, "Chaos in the Colpitts oscillator," *IEEE Trans. Circuits Syst. I, Fundam. Theory Appl.*, vol. 41, no. 11, pp. 771–774, Nov. 1994.

[36] A. M. Shigaev, B. S. Dmitriev, Y. D. Zharkov, and N. M. Ryskin, "Chaotic dynamics of delayed feedback klystron oscillator and its control by external signal," *IEEE Trans. Electron Devices*, vol. 52, no. 5, pp. 790–797, May 2005.

[37] S. V. Grishin, V. S. Grishin, D. V. Romanenko, and Y. P. Sharaevskii, "An ultrawideband spin-wave medium-power chaos generator based on field-effect transistors," *Tech. Phys. Lett.*, vol. 40, no. 10, pp. 853–856, Oct. 2014.

[38] J. N. Blakely, J. D. Holder, N. J. Corron, and S. D. Pethel, "Simply folded band chaos in a VHF microstrip oscillator," *Phys. Lett. A*, vol. 346, nos. 1–3, pp. 111–114, Oct. 2005.

[39] G. Kandiban, S. Manimaran, and A. V. Balachandran, "Chaotic phenomena in a simple 3D autonomous circuit with a diode pair," *Acta Phys. Polonica-Ser. A Gen. Phys.*, vol. 121, no. 3, p. 586, Mar. 2012.

[40] Q. Xu and B. C. Bao, "Simplified Chua's attractor via bridging a diode pair," *J. Eng.*, vol. 4, pp. 125–127, Apr. 2015.

[41] J. Kengne, N. Tsafack, and L. K. Kengne, "Dynamical analysis of a novel single Op-amp based autonomous LC oscillator: Antimonotonicity, chaos, and multiple attractors," *Int. J. Dyn. Control*, vol. 6, no. 4, pp. 1543–1557, Dec. 2018.

[42] J. Liu, J. Ma, J. Lian, P. Chang, and Y. Ma, "An approach for the generation of an nth-order chaotic system with hyperbolic sine," *Entropy*, vol. 20, no. 4, p. 230, Mar. 2018.

[43] M. F. Tsotsop, J. Kengne, G. Kenne, and Z. T. Njitacke, "Coexistence of multiple points, limit cycles, and strange attractors in a simple autonomous hyperjerk circuit with hyperbolic sine function," *Complexity*, vol. 2020, pp. 1–24, Jul. 2020.

[44] T. F. Fozin, P. M. Ezhilarasu, Z. N. Tabekoueng, G. D. Leutcho, J. Kengne, K. Thamilmaran, A. B. Mezatio, and F. B. Pelap, "On the dynamics of a simplified canonical Chua's oscillator with smooth hyperbolic sine nonlinearity: Hyperchaos, multistability and multistability control," *Chaos, Interdiscipl. J. Nonlinear Sci.*, vol. 29, no. 11, Nov. 2019, Art. no. 113105.

[45] M. Joshi and A. Ranjan, "An autonomous chaotic and hyperchaotic oscillator using OTRA," *Anal. Integr. Circuits Signal Process.*, vol. 101, no. 3, pp. 401–413, Dec. 2019.

[46] M. Joshi and A. Ranjan, "New simple chaotic and hyperchaotic system with an unstable node," *AEU-Int. J. Electron. Commun.*, vol. 108, pp. 1–9, Aug. 2019.

[47] F. Yu, H. Shen, L. Liu, Z. Zhang, Y. Huang, B. He, S. Cai, Y. Song, B. Yin, S. Du, and Q. Xu, "CCII and FPGA realization: A multistable modified fourth-order autonomous Chua's chaotic system with coexisting multiple attractors," *Complexity*, vol. 2020, pp. 1–17, Mar. 2020.

[48] A. Tutueva, L. Moysis, V. Rybin, A. Zubarev, C. Volos, and D. Butusov, "Adaptive symmetry control in secure communication systems," *Chaos, Solitons Fractals*, vol. 159, Jun. 2022, Art. no. 112181.

[49] I. Pehlivan, I. M. Moroz, and S. Vaidyanathan, "Analysis, synchronization and circuit design of a novel butterfly attractor," *J. Sound Vibrat.*, vol. 333, no. 20, pp. 5077–5096, Sep. 2014.

[50] M. S. Azzaz, C. Tanougast, S. Sadoudi, and A. Bouridane, "Synchronized hybrid chaotic generators: Application to real-time wireless speech encryption," *Commun. Nonlinear Sci. Numer. Simul.*, vol. 18, no. 8, pp. 2035–2047, Aug. 2013.

[51] S. Vaidyanathan, C. K. Volos, K. Rajagopal, I. M. Kyprianidis, and I. N. Stouboulos, "Adaptive backstepping controller design for the anti-synchronization of identical WINDMI chaotic systems with unknown parameters and its SPICE implementation," *J. Eng. Sci. Technol. Rev.*, vol. 8, no. 2, pp. 1–9, Mar. 2015.

[52] L. Huang, Z. Zhang, J. Xiang, and S. Wang, "A new 4D chaotic system with two-wing, four-wing, and coexisting attractors and its circuit simulation," *Complexity*, vol. 2019, pp. 1–13, Oct. 2019.

[53] J. P. Singh and B. K. Roy, "Multistability and hidden chaotic attractors in a new simple 4-D chaotic system with chaotic 2-torus behaviour," *Int. J. Dyn. Control*, vol. 6, no. 2, pp. 529–538, Jun. 2018.

[54] L. Gong, R. Wu, and N. Zhou, "A new 4D chaotic system with coexisting hidden chaotic attractors," *Int. J. Bifurcation Chaos*, vol. 30, no. 10, Aug. 2020, Art. no. 2050142.

[55] Q. Lai, T. Nestor, J. Kengne, and X.-W. Zhao, "Coexisting attractors and circuit implementation of a new 4D chaotic system with two equilibria," *Chaos, Solitons Fractals*, vol. 107, pp. 92–102, Feb. 2018.

[56] J. Kengne, "Coexistence of chaos with hyperchaos, period-3 doubling bifurcation, and transient chaos in the hyperchaotic oscillator with gyrators," *Int. J. Bifurcation Chaos*, vol. 25, no. 4, Apr. 2015, Art. no. 1550052.

[57] A. Tamasevicius, A. Namajunas, and A. Cenys, "Simple 4D chaotic oscillator," *Electron. Lett.*, vol. 32, no. 11, pp. 957–958, 1996.

[58] T. F. Fozin, J. Kengne, and F. B. Pelap, "Theoretical analysis and adaptive synchronization of a 4D hyperchaotic oscillator," *J. Chaos*, vol. 2014, pp. 1–15, Feb. 2014.

[59] H. P. Chen, S. F. Wang, Y. T. Ku, and M. Y. Hsieh, "Quadrature oscillators using two CFOAs and four passive components," *IEICE Electron. Exp.*, vol. 12, Jan. 2015, Art. no. 20141148.

[60] E. Yuce and S. Minaei, "A modified CFOA and its applications to simulated inductors, capacitance multipliers, and analog filters," *IEEE Trans. Circuits Syst. I, Reg. Papers*, vol. 55, no. 1, pp. 266–275, Feb. 2008.

[61] M. Siripruchyanun, C. Chanapromma, P. H. Silapan, and W. Jaikla, "BiCMOS current-controlled current feedback amplifier (CC-CFA) and its applications," *WSEAS Trans. Electron.*, vol. 5, no. 6, pp. 203–219, Jun. 2008.

[62] A. Singh, M. K. Jain, and S. Wairya, "Novel lossless grounded and floating inductance simulators employing a grounded capacitor based on CC-CFA," *J. Circuits, Syst. Comput.*, vol. 28, no. 6, Jun. 2019, Art. no. 1950093.

[63] N. Herencsar, "Balanced-output CCCFOA and its utilization in grounded inductance simulator with various orders," in *Proc. 41st Int. Conf. Telecommun. Signal Process. (TSP)*, Jul. 2018, pp. 1–5.

[64] A. S. Elwakil and M. P. Kennedy, "Construction of classes of circuit-independent chaotic oscillators using passive-only nonlinear devices," *IEEE Trans. Circuits Syst. I, Fundam. Theory Appl.*, vol. 48, no. 3, pp. 289–307, Mar. 2001.

[65] G. Kenfack and A. Tiedeu, "Secured transmission of ECG signals: Numerical and electronic simulations," *J. Signal Inf. Process.*, vol. 4, no. 2, pp. 158–169, 2013.

GARIMA SHUKLA received the B.Tech. degree in electronics and communication engineering from S. V. C. E., Indore, and the M.Tech. degree in embedded system and VLSI design from S. V. V. V., Indore. She is currently the Ph.D. Research Scholar with the Department of Electronics Engineering, Indian Institute of Technology (Indian School of Mines), Dhanbad. Her research interests include analog VLSI circuit design using the current mode approach and CMOS analog signal processing.

SAJAL K. PAUL received the B.Tech., M.Tech., and Ph.D. degrees in radio physics and electronics from the Institute of Radio Physics and Electronics, University of Calcutta. He has served at Webel Telecommunication Industries, Kolkata; Indira Gandhi National Open University (IGNOU), Kolkata; Advanced Training Institute for Electronics and Process Instrumentation (ATI-EPI), Hyderabad; North Eastern Regional Institute of Science and Technology (NERIST), Nirjuli; and Delhi College of Engineering (DCE), Delhi, in various capacities. He has served the Department of Electronics Engineering, Indian Institute of Technology (Indian School of Mines), Dhanbad, as the Head of the Department and the Dean (Faculty), where he is currently a Professor. He has more than 142 research publications in international and national journals of repute and conferences. His research interests include microelectronic devices, electronic properties of semiconductor, and bipolar and MOS analog integrated circuits.